

Changing the order of a dynamical phase transition through fluctuations in a quantum p -spin model.

Lorenzo Correale^{1,2} and Alessandro Silva¹

¹*SISSA — International School for Advanced Studies, via Bonomea 265, I-34136 Trieste, Italy*

²*INFN — Istituto Nazionale di Fisica Nucleare, Sezione di Trieste, I-34136 Trieste, Italy*

(Dated: August 14, 2023)

We study the non-equilibrium phase diagram of a fully-connected Ising p -spin model, for generic $p > 2$, and investigate its robustness with respect to the inclusion of spin-wave fluctuations, resulting from a ferromagnetic, short-range spin interaction. In particular, we investigate the dynamics of the mean-field model after a quantum quench: we observe a new dynamical phase transition which is either first or second order depending on the even or odd parity of p , in stark contrast with its thermal counterpart which is first order for all p . The dynamical phase diagram is qualitatively modified by the fluctuations introduced by a short-range interaction which drive the system always towards various paramagnetic phases determined by the strength of time dependent fluctuations of the magnetization.

PACS numbers: 05.30.Rt, 64.60.Ht, 75.10.Jm

I. INTRODUCTION

Equilibrium phase transitions, either at zero or finite-temperature, are known to leave a substantial imprint in the nonequilibrium dynamics of a quantum many-body system [1]. For example, even when a stationary state attained after a quantum quench does not reveal signatures of order as in low-dimensional systems [2–4], a linear ramp through a second order quantum critical point leaves universal signatures in the scaling of the number of excitations with the ramp speed [5–8], as confirmed extensively in a number of experiments [9–15]. Analogous signatures are left when a first-order quantum phase transition is crossed [16–18] through the nucleation of resonant bubbles of the new phase close to the critical point [19–21] which leads to a modified Kibble-Zurek-like power-law scaling [22].

Among the signatures of criticality observed out-of-equilibrium, Dynamical Phase Transitions (DPT) occupy a special place. A dynamical quantum criticality can be observed as singular temporal behavior of the Loschmidt echo (LE) most notably after a quench across a quantum phase transition [23–25], even in situations where long-range order cannot be sustained in stationary states. In systems with long-range interactions, on the contrary, intertwined with the singular behavior of the LE [26–31], a standard Landau-type critical behavior based on the dependence of a time-averaged order parameter with respect to the quench parameters can be observed [32, 33]. Peculiar to the second-order dynamical transitions arising in these models is the fact that they are associated to critical trajectories with a divergent time scale in the dynamics separating revivals with a finite order parameter [26]. In the presence of fluctuations critical trajectories become unstable and second order dynamical critical points widen up into chaotic dynamical phases [34–37].

While a great deal is known about second-order dynamical phase transitions, the dynamics of systems displaying equilibrium first order transitions is much less explored. The notion of dynamical criticality associated to the LE has been extended to include first order behavior [38] while first-order and dissipative phase transitions in infinite range p -spin systems coupled to an external bath have been studied in Ref.[39]. However, dynamical transitions occurring in systems displaying first order equilibrium transitions are much less studied.

In this work we address this issue by studying dynamical phase transitions and their stability against fluctuations in a system displaying a first order equilibrium transition: a spin system with infinite range p -spin interactions in a transverse field. We show that, already at mean-field level where the dynamics is effectively classical, the system undergoes a DPT after a quench of the transverse field g , whose order depends non-trivially on p , despite its equilibrium counterpart being always of first order. In particular, we show that the order of the dynamical transition can be inferred entirely from the profile of the underlying energy landscape. We then perturb the model by a short-range two-body interaction tuning the strength of spin fluctuations [34, 35, 40]. While for $p = 2$ a chaotic dynamical region opens up near mean-field criticality [34, 35], we show that for $p > 2$ dynamical chaos is almost entirely replaced by a new prethermal regime, which we define as "dynamical paramagnetic phase", which appears for sufficiently large short-range coupling. This is due to the emission of energy in the form of spin-waves, which predominantly drive the system into a paramagnetic minimum even in the presence of other minima in the energy landscape.

II. MEAN-FIELD DYNAMICS

Let us start by studying the dynamics of N spins $1/2$ subject to all-to-all p -body and a global transverse field

g [41, 42]. Its Hamiltonian is defined as

$$\hat{H}_0 = -\frac{\lambda}{2N^{p-1}} \sum_{i_1 \dots i_p=1}^N \sigma_{i_1}^x \dots \sigma_{i_p}^x - \frac{g}{2} \sum_i \sigma_i^z \quad (1)$$

where σ_i^α are the Pauli matrices at site i . The fully connected p -spin model, which was originally introduced in the context of spin-glasses [41, 42], plays a central role for studies on quantum annealing [43, 44]: its zero-temperature phase diagram can be derived analytically [43–46] and displays a quantum phase transition driven by g , continuous for $p = 2$ and of the first-order for $p > 2$ [43, 46]. In the following we will first address its dynamics and dynamical phase transitions.

A. Semi-classical theory for the post-quench dynamics

We explore the dynamics of the average magnetization $\vec{S}(t) = \langle \sum_j \vec{\sigma}_j(t) \rangle / N = \langle \vec{\sigma}_{k=0}(t) \rangle / N$ following a quench in the transverse field g . The initial state is a ferromagnetic ground state of the Hamiltonian in eq. (1) at $g_0 = 0$, represented as $|\psi_0\rangle = |\rightarrow \dots \rightarrow\rangle$.

The dynamics of $\vec{S}(t)$ is obtained by taking the average over the state $|\psi_0\rangle$ of the Heisenberg equations of motion generated by the Hamiltonian in eq. (1). In the thermodynamic limit $N \rightarrow \infty$, the dynamics becomes effectively classical and the Heisenberg equations for $\vec{S}(t)$ become the following Hamilton equations of motion (see also [39, 47]):

$$\partial_t \vec{S} = \nabla \mathcal{H}_{cl}(\vec{S}, g) \wedge \vec{S}, \quad (2)$$

with initial condition $\vec{S}(0) = \hat{\mathbf{x}}$. The effective potential $\mathcal{H}_{cl}(\vec{S}, g)$ appearing on the right-hand side of eq. (2) is given by

$$\mathcal{H}_{cl}(\vec{S}, g) = -\lambda(S^x)^p - gS^z \quad (3)$$

and the gradient operator ∇ represents the three-dimensional derivative with respect to the collective variable \vec{S} , that is $\nabla = (\frac{\partial}{\partial S_x}, \frac{\partial}{\partial S_y}, \frac{\partial}{\partial S_z})$. The right-hand side of eq. (2) is obtained by replacing the average commutator $\langle [\sum_j \vec{\sigma}_j, \hat{H}_0] \rangle / (i\hbar N)$ with the Poisson parenthesis $\{\vec{S}, \mathcal{H}_{cl}(\vec{S}, g)\} = \nabla \mathcal{H}_{cl}(\vec{S}, g) \wedge \vec{S}$. In the $N \rightarrow \infty$ limit, this substitution becomes exact for every all-to-all interacting spin model, as derived from the general theory developed in Ref. [32]. As the modulus of the magnetization is a constant of motion, the classical dynamics obtained by the procedure described above takes place on the Bloch sphere, defined by the constraint $|\vec{S}|^2 = 1$. Thus, the system under consideration is always in a non-equilibrium state, as all microscopic spins perform a coherent, undamped precession under the dynamics described by Eq. (2).

The dynamics described by eq. (2) is also strongly influenced by the shape of the effective potential $\mathcal{H}_{cl}(\vec{S}, g)$. Depending on the value of p and for sufficiently small values of g , the profile $\mathcal{H}_{cl}(\vec{S}, g)$ on the sphere exhibits various topologies, characterized by the number and positions of its maxima and minima. A deeper discussion on this topic is available in Appendix A. Specifically, for $p = 2$, we observe two symmetric minima separated by a maximum at the North pole ($\vec{S} = \hat{\mathbf{z}}$). For $p \geq 3$ odd, the same topology persists, but the profile becomes asymmetric with respect to the North pole. Conversely, for $p \geq 4$ even, the potential features three minima: one at the North pole and two symmetric minima with respect to it. Consequently, by slicing the sphere along meridians that intercept the minima, we obtain three possible shapes for $\mathcal{H}_{cl}(\vec{S}, g)$, each corresponding to a different value of p :

- a symmetric double-well for $p = 2$
- an asymmetric double-well for $p \geq 3$ (odd), with one paramagnetic and one ferromagnetic minimum.
- a symmetric triple-well for $p \geq 4$ (even), with one paramagnetic minimum and two opposite ferromagnetic minima.

It is worth noting that these profiles qualitatively change for $g > g_{sp} = p(p-2)^{(p-2)/2} / (p-1)^{(p-1)/2}$, commonly referred to as the *spinodal point* [44], where $\mathcal{H}_{cl}(\vec{S}, g)$ becomes a single-well centered around $\vec{S} = \hat{\mathbf{z}}$.

The dynamics of $\vec{S}(t)$, initiated from the fully polarized state $\vec{S}(0) = \hat{\mathbf{x}}$, [48], exhibits qualitatively different orbits, depending on the value of the post-quench transverse field g , as depicted in Fig. 1:

1. Below a certain threshold, $g < g_{dyn}$ (trajectory (a)), the dynamics commences from a ferromagnetic well (since $g < g_{sp}$, see also Appendix A), and the initial energy is insufficient to surmount the nearest maximum at $S^x = S_m^x(g)$. Consequently, the magnetization oscillates around the ferromagnetic minimum, with $S^x(t) > S_m^x(g)$.
2. For $g > g_{dyn}$ (trajectory (b)), the system possesses enough energy to explore the entire landscape.
3. At precisely $g = g_{dyn}$ (trajectory (c)), the system has sufficient energy to reach the top of the barrier but is unable to surpass it. Here the period of the oscillations, $T_{cl}(g)$, diverges (see Appendix B for further details), and the magnetization approaches the local maximum infinitely slowly. The resulting orbit forms a separatrix.

The three cases listed above correspond to three different possible topologies for the underlying orbits at large times. In the spirit of Ref. [49], we classify each distinct topology as a *dynamical phase*. Consequently,

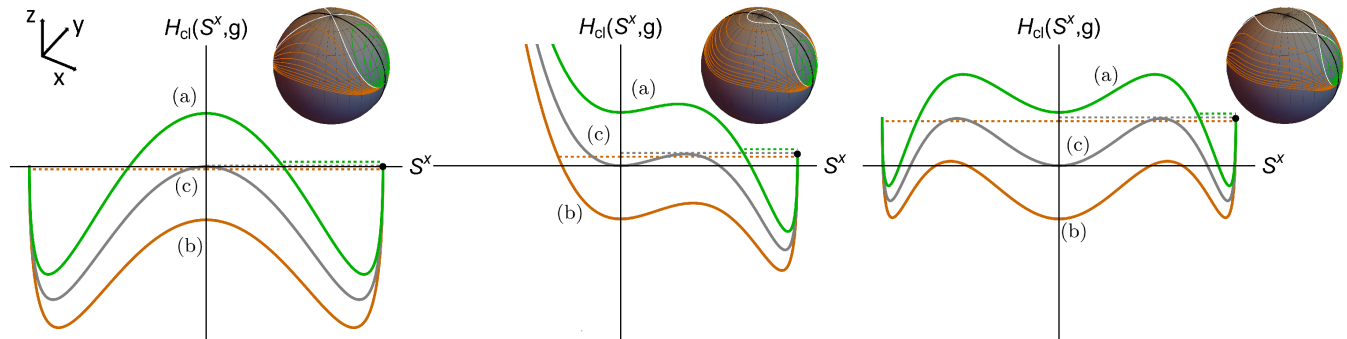


FIG. 1. Energy profiles described by the equation (3), for several values of g and for $p = 2$ (left), $p = 2n + 1$ (center) and $p = 2n + 2$ (right), respectively, with $n \geq 1$. All the three profiles lie in the plane $S^y = 0$ (black cut on the Bloch spheres, where $S^z = \sqrt{1 - (S^x)^2}$). Depending on the post quench values of the transverse field g , orbits starting from $S^x(0) = 1$ display qualitatively different behaviours: they are either confined in a single well (a) or explore the whole landscape (b), for values of g respectively below and above a dynamical critical point g_{dyn} . Exactly at $g = g_{dyn}$, the system lies on a separatrix (c) with diverging period. See also the orbits in Fig. 2 (a) and (d) for a comparison.

the singular dynamics at $g = g_{dyn}$ leads to a DPT. From a practical point of view, the DPT can be studied also in terms of a "dynamical order parameter", such as the time-averaged longitudinal magnetization $\overline{S^x} = \lim_{T \rightarrow \infty} \int_0^T dt S^x(t) / T$: for $g \rightarrow g_{dyn}$, the change of topology in the orbits is signalled by a divergence in of their period $T_{cl}(g)$, in turn creating a non-analyticity in the function $\overline{S^x}(g)$. In particular, both $T_{cl}(g)$ and $\overline{S^x}(g)$ display a log-singularity while approaching the dynamical transition (as shown in Appendix B), a feature already known for other mean-field models driven away from equilibrium [32, 50]. It is important to note that such a DPT can be observed in the $N \rightarrow \infty$ limit only: for a finite size, quantum fluctuations are restored and induce dephasing between local spins, leading to the relaxation of physical observables to their thermodynamic expectation value [35].

The nature of the mean-field DPT is qualitatively influenced by the interplay between various stationary points, which depends solely on the parity of p . Therefore, in the following, we focus on studying Eq. (2) for $p = 3$ and 4. These cases, together with $p = 2$, are paradigmatic and represent the three possible shapes of the landscape listed above, respectively.

B. The dynamical transition

The first observation to make is that, the order of a DPT is not necessarily the same of the thermal equilibrium phase transition displayed for the p -spin model for the same value of p . The case $p = 2$ is special, as it displays a thermal phase transition [51] and a dynamical phase transition which are both of the second order [26, 32, 45]. The dynamical one is detected by $\overline{S^x}$ which, for a symmetry breaking initial condition $\vec{S}(0)$,

is finite for $g < \lambda$ and vanishes for $g > \lambda$ (due to the symmetry of the two wells), corresponding respectively to *dynamical ferromagnetic* and *dynamical paramagnetic* phases. The continuity of this DPT is not a consequence of the symmetry of $\mathcal{H}_{cl}(\vec{S}, g)$ under the reflection $S^x \rightarrow -S^x$, but it is rather a general property related to the topology of the phase space. Indeed, when g approaches g_{dyn} both from above and below, the energy of the orbit gets close to the one of the separatrix, which has a crossing at the only local maximum of $\mathcal{H}_{cl}(\vec{S}, g_{dyn})$. Every dynamics starting on the separatrix approaches asymptotically this maximum in \vec{S}_c ($\vec{S}_c = \hat{z}$ for $p = 2$), i.e.

$$\lim_{t \rightarrow \infty} \vec{S}(t) = \vec{S}_c \quad (4)$$

The orbits asymptotically close to the separatrix, retrieved for $g \rightarrow g_{dyn}^{\pm}$ develop a plateau at \vec{S}_c whose length diverges with the period $T_{cl}(g)$, so that

$$\lim_{g \rightarrow g_{dyn}^{\pm}} \overline{S^x}(g) = S_c^x \quad (5)$$

and the dynamical transition is continuous.

For $p > 2$, the results summarized Fig. 2 always show the emergence of a DPT at some $g = g_{dyn}$ (such that g_{dyn} is below the spinodal point g_{sp} for every p), whose qualitative features depend on the parity of p , unlike its static counterpart. For $p = 3$ the topology of the phase space is the one of a double well like in the case of $p = 2$ (though without \mathbb{Z}_2 symmetry), hence the transition is continuous, by the same argument made for $p = 2$. In particular, a dynamical ferromagnetic phase is again retrieved for some $g < g_{dyn}$, where all the orbits are confined in a ferromagnetic well (green trajectories, Fig.2-(a)), while for $g > g_{dyn}$ the to oscillations of the orbits between the two wells (orange trajectories, Fig.2-(a)) lead to the emergence of a *dynamical bistable*

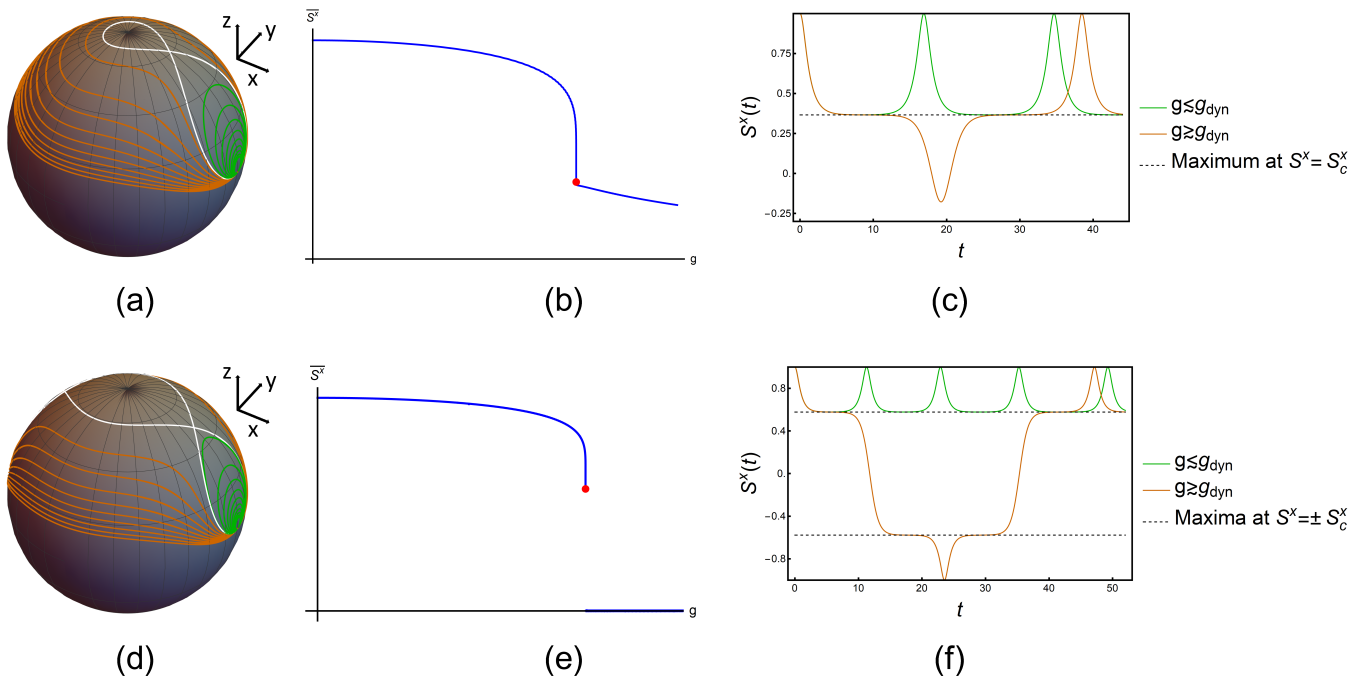


FIG. 2. (Color online) From left to right, we plot the orbits of the magnetization on the Bloch sphere, described after a quench starting in $S^x(0) = 1$ ((a) and (d)), the corresponding time-averaged magnetization $\overline{S^x}$ ((b) and (e)) and the behaviour of $S^x(t)$ near the critical point ((c) and (f)). The plots on the upper row corresponds to the case of $p = 3$, the ones below to $p = 4$. **(Left)** For both values of p , the system evolves on trajectories which either are confined in a ferromagnetic well (green), for $g < g_{dyn}$, or enclose all the local minima (orange), for $g > g_{dyn}$. The two regions are divided by a critical trajectory (white), corresponding to $g = g_{dyn}$. **(Center)** Plot of the dynamical order parameter $\overline{S^x}$ as a function of g . At the critical point (red dot), this is continuous for $p = 3$ only. **(Right)** Behaviour of the longitudinal magnetization for $g \simeq g_{dyn}$: for $p = 3$, $S^x(t)$ exhibits a plateau at the only maximum in $S^x_m(g_{dyn}) = S^x_c$ (of the landscape $\mathcal{H}_{cl}(\vec{S}, g_{dyn})$), both above and above the transition; for $p = 4$, the dynamics is characterized by a single plateau above g_{dyn} and two, symmetric plateaus below g_{dyn} .

phase, where $\overline{S^x}$ is a weighted average of the two minima that varies continuously with g and exhibits a cusp at $g = g_{dyn}$. The argument relating the continuity of $\overline{S^x}$ to the presence of a single unstable stationary point is shown in Fig. 2-(c), showing the plateaus developed by the trajectories near g_{dyn} , both for $g < g_{dyn}$ (green plot) and $g > g_{dyn}$ (orange plot).

The situation changes, due to a drastic change in the phase space topology, for $p = 4$: while approaching the critical point from below, the dynamics is confined in the rightmost ferromagnetic sector and $\overline{S^x}$ still tends to a local maximum S^x_c (green trajectories, Fig. 2-(d)), which is nonvanishing (see App. A and B for further details); moving even slightly above the transition point the trajectories become symmetric with respect to the $y - z$ plane (orange trajectories, Fig. 2-(d)), as the stationary points of $\mathcal{H}_{cl}(\vec{S}, g)$ are, hence $\overline{S^x} = 0$. In a more general perspective, we see that the important topological feature here is the presence of *two maxima* of $\mathcal{H}_{cl}(\vec{S}, g_{dyn})$ with the same energy, at $S^x = \pm S^x_c$, where the separatrix (white trajectory in Fig. 2-(d)) has a crossing. As a consequence, slightly below or above the transition, $S^x(t)$ respectively exhibits plateaus of diverging length

in proximity of the positive maximum or symmetrically near the two maxima (see respectively green and orange plot in Fig. 2 (f)), creating a discontinuity in $\overline{S^x}$.

III. NON-EQUILIBRIUM SPIN WAVE DYNAMICS

A. Non-equilibrium spin-wave theory

The dynamical transitions studied in Sec. II arise from the coherent dynamics performed by the local spins in the $N \rightarrow \infty$ limit, where they are effectively decoupled from each other due to the all-to-all interaction among them. This phenomenon is expected to be unstable with respect to the inclusion of fluctuations in the dynamics, which lead the system to eventually thermalize. However, if the coupling between the magnetization and fluctuations is not too large, the amplitude of fluctuations is expected to be small for a parametrically long time, leaving possible instances of dynamical phases in the *prethermal* stage of the dynamics [52–54].

This possibility was investigated in Ref.,[34] using the

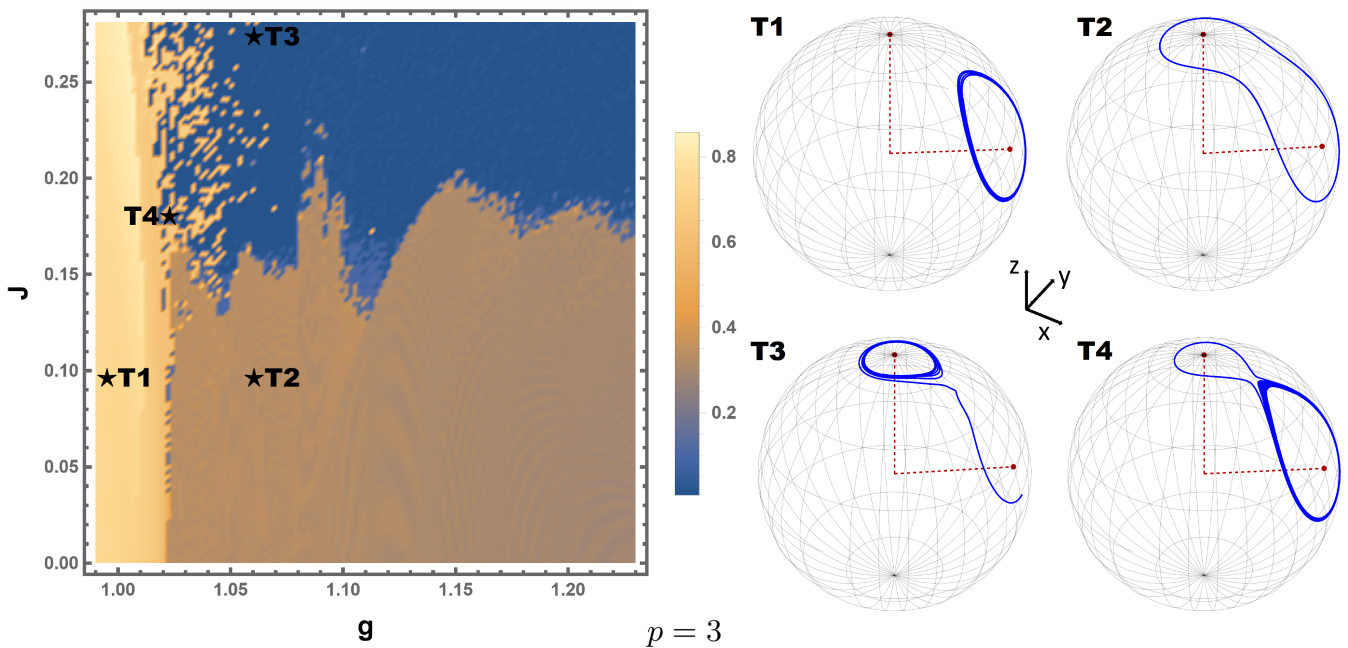


FIG. 3. (Color online) Non-equilibrium phase diagram of the p -spin model Eq.(1), for $p = 3$, obtained integrating simultaneously equations Eq.(8) and (10) for a quench, starting from the fully polarized state $S^x(0) = 1$, up to time $T = 2000$ and for the set of values of g and J specified on the axes (here we posed $N = 100$ and $\lambda = 1$). The color of each point on the phase diagram corresponds to a value of the time-averaged magnetization $\overline{S^x}$, as specified in the interval shown on the right of the diagram. In particular, the yellow and the orange regions correspond to dynamical ferromagnetic and paramagnetic phases, respectively, where the orbits are either confined in the ferromagnetic well (plot T1) or encircle both the two minima (plot T2). In the blue region, instead, is the dynamical paramagnetic region where the magnetization revolves around the minimum on the North pole (plot T3); here $\overline{S^x}$ is closer to 0 than in any other phase, though non-vanishing, and increases discontinuously when moving across the border with the orange zone. The crossover region is instead a narrow chaotic phase, reminiscent of the one found in [34], where collective spin can localize at large times in either the paramagnetic or the ferromagnetic minima (plot T4).

non-equilibrium spin-wave theory (NEQSWT), where it was shown that, for $p = 2$, the dynamical critical point retrieved at the mean-field level is melted into an entire chaotic region of the phase diagram when fluctuations are included. Here we use the NEQSWT to perform the same analysis in the more general case of $p > 2$, considering the quench dynamics of the p -spin model under the influence of an extra, short-range term in the Hamiltonian. We assume that our system is on a one-dimensional lattice with periodic boundary conditions, and the short-range interaction term is expressed as in the spirit of Ref. [34]: $\hat{U} = -J \sum_i \sigma_i^x \sigma_{i+1}^x + J (\sum_i \sigma_i^x)^2 / N$. In momentum space, this can be expressed as:

$$\hat{U} = -\frac{J}{N} \sum_{k \neq 0} \cos k \tilde{\sigma}_k^x \tilde{\sigma}_{-k}^x \quad (6)$$

where k is an integer multiple of $2\pi/N$, N being the system size. We leave out the term with $k = 0$, given by $J(\sum_i \sigma_i^x)^2 / N$, which does not create fluctuations and just modifies the mean-field component (Eq. (1)) of the Hamiltonian. Equation (6) give us the easiest perturbation that breaks the permutation symmetry in eq.(1); nevertheless, as we shall discuss later, all our

results are expected to be independent of the range of interaction and of the dimensionality of the lattice. In the following, we provide a concise summary of the essential steps required for the implementation of NEQSWT, reserving a more comprehensive derivation and technical details for Appendix C.

The fundamental hypothesis underlying NEQSWT is that, at least as long as J is sufficiently small, the net effect of the term from eq. (6) is to give rise to small spin-wave excitations on top of the collective classical spin $\vec{S}(t)$. In particular, when the magnetization length is close to its maximal value, $|\vec{S}(t)| \simeq 1$, the dynamics of $\vec{S}(t)$ can still be effectively described in terms of trajectories close to the Bloch sphere, perturbed by fluctuations induced by the finite k degrees of freedom. Thus, we implement NEQSWT by first rewriting the spin operators in Eq.(1) in a time-dependent, rotating reference frame $\mathcal{R} = (\mathbf{X}(t), \mathbf{Y}(t), \mathbf{Z}(t))$, by applying the rotation $V(\theta(t), \phi(t)) = \exp(-i\phi(t) \sum_i \sigma_i^z / 2) \exp(-i\theta(t) \sum_i \sigma_i^y / 2)$, where the spherical angles $\theta(t)$ and $\phi(t)$ are fixed such that the magnetization $\vec{S}(t)$ is aligned with the Z-axis in

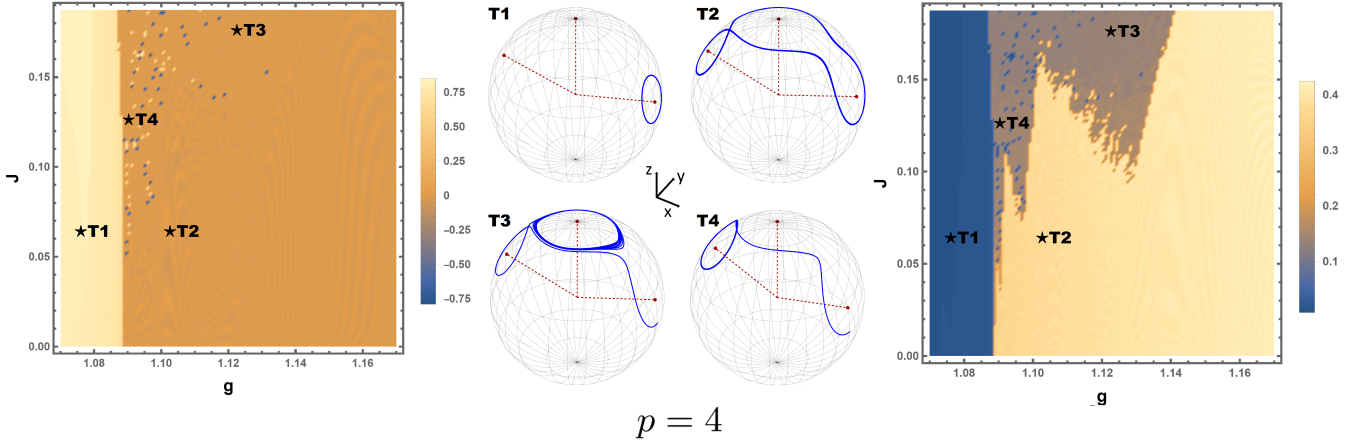


FIG. 4. (Color online) Simultaneous plot of the time-averaged magnetization $\overline{S^x}$ (left) and time-averaged fluctuations $\overline{(\delta S^x)^2}$ (right), for $p = 4$. These are obtained integrating equations Eq.(8) and (10) for the same default parameters of N, λ and the maximum time T listed in the caption of Fig.3. For both the plots, each color corresponds to a value of the observable we plot, as specified in the legends reported on the right of each diagram. **(Left)** From the plot of S^x , we identify two main regions: one corresponds to a dynamical ferromagnetic phase (yellow), where $\overline{S^x} > 0$ (plot T1), while the other is a paramagnetic phase (orange) where $\overline{S^x} = 0$. In between, some "chaotic spots" (blue and yellow spots) are found occasionally, where the magnetization eventually falls in one of the other two symmetric, ferromagnetic minima (plot T4). **(Right)** Looking at the average fluctuations $\overline{(\delta S^x)^2}$, we clearly see that the in dynamical paramagnetic region, delimited by a white line, can be split in a sub-phase 1 (yellow), where the dynamical trajectories either surround symmetrically all the three minima of the landscape (plot T2) and a sub-phase 2 (blue), where the magnetization localizes (predominantly) in a paramagnetic well (plot T3). The border between the two identifies the transition line $J = J_{dyn}(g)$.

the new frame, for any $t > 0$. Then, assuming that the fluctuations transverse to $\mathbf{Z}(t)$ are small, we expand the spin variables in the new frame \mathcal{R} using the Holstein-Primakoff (HP) transformation [55]:

$$\begin{aligned} \sigma_i^X &\simeq q_i/\sqrt{s}, & \sigma_i^Y &\simeq p_i/\sqrt{s}, \\ \sigma_i^Z &= 1 - \frac{q_i^2 + p_i^2 - 1}{2s}, \end{aligned} \quad (7)$$

where $s = 1/2$ for the current case. We retain perturbative terms in the spin-wave modes $(\tilde{q}_k, \tilde{p}_k)$, i.e., the Fourier transform of (q_i, p_i) , at the leading order only. In our case, this amounts to retain only terms in Eq.(1) that are quadratic in \tilde{q}_k and \tilde{p}_k . Then, the evolution of the spherical angles is determined by the self-consistent equations $S^X(t) = S^Y(t) = 0$, which in our analysis read as:

$$\begin{cases} s\dot{\phi} = p\lambda(\sin\theta)^{p-2}(\cos\phi)^p \cos\theta \{1 - (p-1)\epsilon(t)\} - g \\ \quad - 2J\delta^{qq}(t) \cos\theta \cos^2\phi + 2J\delta^{qp}(t) \sin\phi \cos\phi \\ s\dot{\theta} = p\lambda(\sin\theta \cos\phi)^{p-1} \sin\phi \{1 - (p-1)\epsilon(t)\} + \\ \quad - 2J\delta^{pp}(t) \sin\theta \sin\phi \cos\phi \\ \quad + 2J\delta^{qp}(t) \sin\theta \cos\theta \cos^2\phi \end{cases} \quad (8)$$

where

$$\delta^{\alpha\beta}(t) \equiv \sum_{k \neq 0} \Delta_k^{\alpha\beta}(t) \cos k/(Ns), \quad (9)$$

for $\alpha, \beta \in \{p, q\}$, is the "quantum feedback" by which the classical spin gets coupled to the corresponding spin-wave

correlation functions, defined by

$$\begin{aligned} \Delta_k^{qq}(t) &\equiv \langle \tilde{q}_k(t) \tilde{q}_{-k}(t) \rangle, & \Delta_k^{pp}(t) &\equiv \langle \tilde{p}_k(t) \tilde{p}_{-k}(t) \rangle, \\ \Delta_k^{qp}(t) &\equiv \langle \tilde{q}_k(t) \tilde{p}_{-k}(t) + \tilde{p}_k(t) \tilde{q}_{-k}(t) \rangle / 2, \end{aligned}$$

and evolving according to the linear differential equations of motion

$$\begin{cases} s \frac{d}{dt} \Delta_k^{qq} = (4J \cos k \cos \theta \sin \phi \cos \phi) \Delta_k^{qq} \\ \quad + \{2p\lambda(\sin \theta)^{p-2}(\cos \phi)^p - 4J \cos k \sin^2 \phi\} \Delta_k^{qp} \\ s \frac{d}{dt} \Delta_k^{qp} = -\{p\lambda(\sin \theta)^{p-2}(\cos \phi)^p \\ \quad - 2J \cos k \cos^2 \phi \cos^2 \theta\} \Delta_k^{qq} \\ \quad + \{p\lambda(\sin \theta)^{p-2}(\cos \phi)^p - 2J \cos k \sin^2 \phi\} \Delta_k^{pp} \\ s \frac{d}{dt} \Delta_k^{pp} = -\{2p\lambda(\sin \theta)^{p-2}(\cos \phi)^p \\ \quad - 4J \cos k \cos^2 \phi \cos^2 \theta\} \Delta_k^{qp} \\ \quad - (4J \cos k \cos \theta \sin \phi \cos \phi) \Delta_k^{pp} \end{cases} \quad (10)$$

defined for each value of $k = 2\pi n/N$, where $n = 1, \dots, N-1$. We notice that, in the limit of $J \rightarrow 0$, the equations (8) decouple from the quantum feedback and reduce to a representation of equation (2) in the spherical coordinates $\theta(t)$ and $\phi(t)$.

Our expansion is expected to be valid as long as the

density of spin-wave excitations is small, that is

$$\epsilon(t) = \frac{1}{N_s} \sum_{k \neq 0} \frac{\Delta_k^{qq}(t) + \Delta_k^{pp}(t) - 1}{2} \ll 1. \quad (11)$$

In this case, the modulus of the magnetization $|\vec{S}(t)| = 1 - \epsilon(t)$ is close to one the dynamics can still be described in terms of classical trajectories. In this regime, spin waves behave as free bosonic excitations, which interact with the macroscopic collective spin only, corresponding to the $k = 0$ mode. Higher-order terms appearing in eq. (1), which account for nonlinear scattering among the spin waves, can be neglected: they are expected to contribute significantly to the dynamics only at longer times and to drive the system away from the prethermal regime relevant for the DPT discussed here.

B. Modified non-equilibrium phase diagram

The presence of spin-waves opens a channel for internal dissipation: the magnetization $\vec{S}(t)$ is damped by the emission of spin waves, an effect that is behind the disruption of the dynamical critical point for $p = 2$ and the emergence of a chaotic crossover phase instead [34, 35]. It is natural to ask if spin-wave emission is going to have the same effect in the first-order case $p > 2$.

To understand the effects of fluctuation on the mean-field dynamical transition, we study the post-quench dynamics of the system at $J \neq 0$, by simultaneously integrating equations (8) and (10), for a range of values of the couplings g and J . We verify that, for each choice of g and J and at the time-scales explored, the spin wave density $\epsilon(t)$ is small (some examples are shown in Fig. 5), so that the dynamics we study is consistently in a prethermal regime. Before the quench, we again prepare the system in the fully polarized state along the x -direction, so that $\theta(0) = \pi/2$ and $\phi(0) = 0$, and assume that no spin-wave mode is excited, by imposing that $\Delta_k^{qq}(0) = \Delta_k^{pp}(0) = 1/2$ and $\Delta_k^{qp}(0) = 0$. Below we will reconstruct the various dynamical phases by looking at \bar{S}^x as a function of g and J and at individual trajectories. As we study the dynamics for values of g below the spinodal point $g_{sp}(p)$ (defined in Sec.II), the new dynamics is still equivalent to the one of a particle moving in a multi-well shaped energy profile, like mean-field dynamics, with an additional damping due to the exchange of energy with the spin-wave degrees of freedom, the latter acting as a self-generated bath (see Sec.III C for further details).

The exchange of energy between the magnetization and the spin-waves opens the route for the appearance of new dynamical phases. In particular, for the dynamical protocol we described and generic values of g and J , $\epsilon(t)$ grows from zero saturating to a typical small value (see Fig. 5), while the magnetization is correspondingly

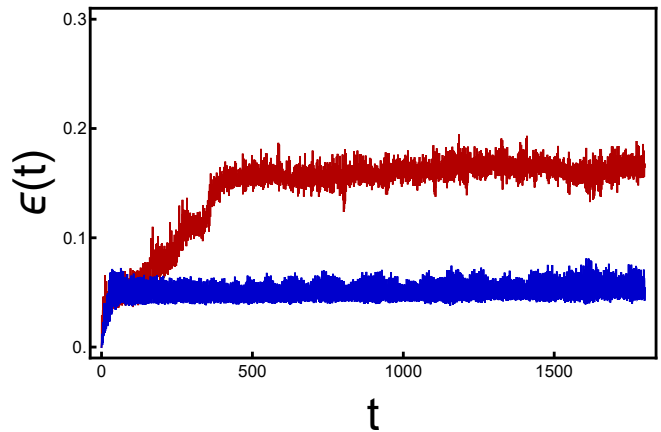


FIG. 5. (Color online) Plots of two examples of the profile of the function $\epsilon(t)$, defined in eq. (11) and computed by within the NEQSW described in the main text, by fixing either $p = 3$, $J = 0.25$, $g = 1.15$ (red plot) or $p = 4$, $J = 0.2$, $g = 1.12$ (blue plot). In both plots we fix $N = 100$ and $\lambda = 1$.

damped from its initial mean-field orbit to another one where the unperturbed energy $\mathcal{H}_{cl}(\vec{S}(t), g)$ is slightly different, possibly even localizing in a single well. We define the new dynamical phases in terms of the topology of the trajectories asymptotically reached after the damping. Once again, we stress that such new dynamical phases are *prethermal* and are expected to be disappear at long-times as soon as the non-linear interaction among the spin-waves degree of freedom is taken into account, leading to thermal relaxation of the system.

If spin waves were emitted at a constant rate in time, the orbits encompassing all the minima (that is, orange trajectories in Fig. 2-(a) and (d)) would localize down one the wells of the effective potential on the Bloch sphere, either the paramagnetic minimum or one of the ferromagnetic minima (a single one for $p \geq 3$ odd or a pair for $p \geq 4$ even), with approximately equal probability. The plot obtained for $p = 3$ in Fig. 3 shows that this is not the case: the dynamical ferromagnetic phase is of course always robust against fluctuations, while the dynamical bistable one is not and for sufficiently large values of J the trajectories localize predominantly around the paramagnetic minimum, asymptotically converging to stable orbits, thus identifying a new *dynamical paramagnetic phase*. Quantitatively, in Fig. 3 we observe three typical asymptotic behaviour for the trajectories (either encompassing all the wells or orbiting around one of the two minima): to each of them corresponds to a narrow interval of values for \bar{S}^x , being greatest in the dynamical ferromagnetic phase and smallest in the paramagnetic one (although non vanishing due to the asymmetry of the energy profile). The dynamical order parameter \bar{S}^x also exhibits a discontinuity when crossing the border line $J_{dyn}(g)$ (discussed in greater detail D), between the dynamical

bistable and paramagnetic regions, giving rise also to a new first-order transition driven by J . The predominance of localization around $S^x = 0$ is softened close to the mean-field critical point $g = g_{dyn}$, where localization in the ferromagnetic basin becomes more frequent and the line limiting the dynamical ferromagnetic phase is melted in a narrow chaotic crossover region, equivalent to the one observed for $p = 2$ [34].

As shown in Fig. 4, a similar phenomenon is observed for $p = 4$, where the collective spin $\vec{S}(t)$, initially oscillating in the mean-field paramagnetic region, suddenly falls into the well around the North pole of the Bloch sphere, as soon as J is moved above a critical threshold $J_{dyn}(g)$. Unfortunately, this discontinuity in the time-evolution can not be appreciated by looking at the average $\overline{S^x}$, displayed in Fig. 4(left), which vanishes for orbits either surrounding all the minima or asymptotically localizing in the paramagnetic well, while showing once again the stability of the dynamical ferromagnetic phase (where $\overline{S^x} > 0$) against fluctuations. Thus, we also examine the behaviour of the time-averaged fluctuation [39], defined as

$$\overline{(\delta S^x)^2} = \lim_{T \rightarrow \infty} \frac{1}{T} \int_0^T dt (S^x(t) - \overline{S^x})^2. \quad (12)$$

The value of $\overline{(\delta S^x)^2}$ depends on the integration parameters g and J and decreases discontinuously as J is again raised above a threshold $J_{dyn}(g)$ (whose values are different from the one found for $p = 3$), as it can clearly be observed in Fig. 4 (right). From the corresponding phase diagram, we see that the dynamical paramagnetic phase, corresponding to $\overline{S^x} = 0$, can be divided in two sub-phases:

- a *dynamical paramagnetic phase 1*, where the orbits surround all the minima, like in the corresponding mean-field phase ;
- a *dynamical paramagnetic phase 2*, where the trajectories eventually localize in the well around the minimum at $\overline{S^x} = 0$.

Specifically, smaller values of $\overline{(\delta S^x)^2}$ correspond to an asymptotic localization in the paramagnetic well.

At the transition line $J_{dyn}(g)$ between the two dynamical paramagnetic phases, $\overline{(\delta S^x)^2}$ is discontinuous (see also Appendix D) and thus we can identify a dynamical transition for $p \geq 4$ even, driven by J , being of the first-order like the one retrieved in the mean-field case. In passing we also observe that, close to the mean-field critical point $g = g_{dyn}$, the dynamical paramagnetic phase 2 is filled with few "chaotic" spots, where the orbits eventually localize instead in one of the two ferromagnetic wells (each of them associated to a different sign of $\overline{S^x}$). These spots become more frequent as we cross over to the dynamical paramagnetic phase retrieved at smaller values of g .

C. The mechanism behind the localization of the magnetization

Our results are very different from the ones found in Ref. [34] for the case of $p = 2$, where the same fluctuations lead to dynamical chaos. In this section we show that, despite the apparent difference, the dynamical phases retrieved both for $p = 2$ and $p > 2$ share a common origin, which can be related to the predominant emission of spin waves when the classical trajectory traverses the paramagnetic well.

Intuitively, the inhomogeneous emission is due to the specific form of the short-range perturbation in eq.(6), which induces fluctuations in the collective dynamics when the local spins are not aligned with the x -axis: as the maximal misalignment in the dynamics is reached when the magnetization is close to the North pole $\vec{S} = \hat{z}$, and in particular close to the plane $S^x = 0$, spin-waves are expected to be mostly emitted there. From a quantitative point of view, it is useful to investigate the spin-wave density rate, which using eq. (11) reads as

$$\frac{d\epsilon(t)}{dt} = \frac{1}{2Ns} \sum_{k \neq 0} \left(\frac{d\Delta_k^{qq}(t)}{dt} + \frac{d\Delta_k^{pp}(t)}{dt} \right) \quad (13)$$

or, using explicitly eqs. (10), as

$$\begin{aligned} \frac{d\epsilon(t)}{dt} &= -4 \frac{J}{s} (\mathbf{X} \cdot \hat{\mathbf{x}})(\mathbf{Y} \cdot \hat{\mathbf{x}}) (\delta^{qq}(t) - \delta^{pp}(t)) + \\ &+ 4 \frac{J}{s} ((\mathbf{X} \cdot \hat{\mathbf{x}})^2 - (\mathbf{Y} \cdot \hat{\mathbf{x}})^2) \delta^{qp}(t) \\ &= 4 \frac{J}{s} \cos \theta \sin \phi \cos \phi (\delta^{qq}(t) - \delta^{pp}(t)) + \\ &+ 4 \frac{J}{s} (\cos^2 \theta \cos^2 \phi - \sin^2 \phi) \delta^{qp}(t), \end{aligned} \quad (14)$$

where the quantum feedback terms $\delta^{\alpha\beta}(t)$ are defined in eq. (9). The emission rate $d\epsilon/dt$ is then determined by the couplings

$$\begin{aligned} C_1(\theta, \phi) &= (\mathbf{X}(t) \cdot \hat{\mathbf{x}})(\mathbf{Y}(t) \cdot \hat{\mathbf{x}}) = \cos \theta \sin \phi \cos \phi \\ C_2(\theta, \phi) &= (\mathbf{X}(t) \cdot \hat{\mathbf{x}})^2 - (\mathbf{Y}(t) \cdot \hat{\mathbf{x}})^2 = \\ &= \cos^2 \theta \cos^2 \phi - \sin^2 \phi \end{aligned} \quad (15)$$

which are independent of p and depend only on the projection of the time-dependent frame \mathcal{R} on the x -axis, along which the local spins interact through the perturbation introduced in eq. (6). In Appendix C, Sec. 3, we also show explicitly that the expression for the coefficients $C_1(\theta, \phi)$ and $C_2(\theta, \phi)$ in eq. (15) depends only on the form of the perturbation in eq. (6). Moreover, from eq.(15) we can see explicitly that $d\epsilon/dt = 0$ when the magnetization is along the x -axis ($\theta = \pi/2$) and that the magnitude of both $C_1(\theta, \phi)$ and $C_2(\theta, \phi)$ is maximised around the North Pole (see Fig. 6, left panels), confirming the intuition that the maximum

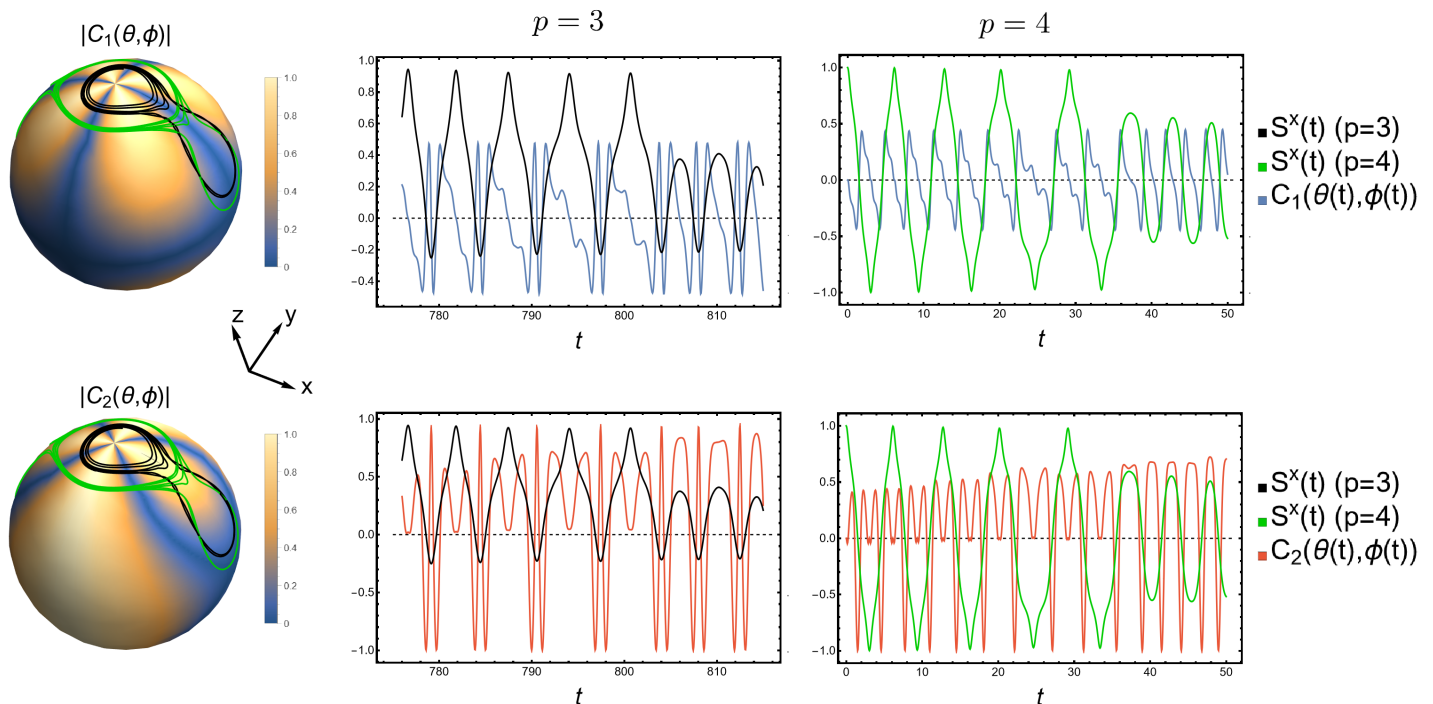


FIG. 6. (Color online) Dynamics of two trajectories, parametrized by $\theta(t)$ and $\phi(t)$ and computed respectively for $p = 3$, $g = 1.09$, $J = 0.26$ (black plots) and $p = 4$, $g = 1.13$, $J = 0.15$ (green plots). **(Left)** Spherical plots of the magnitude of the couplings $C_1(\theta, \phi)$ and $C_2(\theta, \phi)$, against the dynamical evolution of the two trajectories on the Bloch Sphere. **(Center)** Time evolution of the couplings $C_1(\theta(t), \phi(t))$ (blue) and $C_2(\theta(t), \phi(t))$ (red) along the trajectory obtained at $p = 3$, each compared against the longitudinal magnetization $S^x(t) = (1 - \epsilon(t)) \sin \phi(t) \cos \phi(t)$ (black). **(Right)** Same plots represented at the center, this time for the trajectory computed at $p = 4$.

spin-wave emission occurs concomitantly with the maximal misalignment between $\vec{S}(t)$ and $\hat{\mathbf{x}}$. Our intuition is further confirmed by the plots in Fig. 6, where we show the time-evolution of $C_1(\theta, \phi)$ and $C_2(\theta, \phi)$, along two generic classical trajectories, respectively for $p = 3, 4$: when the magnetization visits the ferromagnetic well, both the couplings vanish and no spin-wave is excited, while their magnitude is maximised when the magnetization is close to the plane $S^x = 0$.

As the predominant emission around the North pole is determined only by the short-range perturbation, the different phenomena observed for $p = 2$ and $p > 2$ respectively can be addressed to the different stability properties of the stationary point $\theta = 0$ of the energy landscape in eq.(3): while, for $p = 2$, $\theta = 0$ is unstable and symmetric fluctuations in the two wells [56] induce dynamical chaos [34, 35], for $p > 2$ $\theta = 0$ becomes a stable minimum so that the magnetization moves on stationary orbits after being damped, giving birth to the dynamical paramagnetic regions shown in Fig. 3 (left) and Fig. 4 (right). This phenomenon is reminiscent of Hopf bifurcations [57] occurring in classical dynamical systems.

It is also worth noticing the way by which the fluc-

tuations induce the localization of the collective spin is slightly more subtle than a simple dissipation mechanism. In particular, we observe that when $\epsilon(t) > 0$, the magnetization length is $|\vec{S}(t)| = 1 - \epsilon(t)$ decreases, so that the dynamics in eq.(8) takes place in the time-dependent modified potential

$$\mathcal{H}_{\epsilon(t)}(\theta, \phi) = - (1 - \epsilon(t))^p \{ \lambda (\sin \theta \cos \phi)^p + \frac{g}{(1 - \epsilon(t))^{p-1}} \sin \theta \}, \quad (16)$$

As shown in the animated plots (see Supplemental Material [58]), the profile of the $\mathcal{H}_{\epsilon(t)}(\theta, \phi)$ is squeezed towards zero energy when $\epsilon(t)$ grows: this eventually leads the magnetization to be trapped in the paramagnetic region, where $\epsilon(t)$ exhibits large spikes, while the spin-wave dynamics is nearly stationary across the ferromagnetic wells.

Our results are expected to be independent of the range of interaction of the perturbation in eq.(6) and of the dimensionality of the lattice: replacing the k -dependent couplings $J \cos(k)$ with generic $\tilde{J}_{\mathbf{k}}$ [59] leaves eq. (14) invariant [60] and spin-waves are still expected to be emitted around $\theta = 0$, as explicitly shown for the case of $p = 2$ [35]; on the other hand, introducing a short-range interaction along a direction not coinciding with the x -

axis changes the couplings in eq.(15) and spin-wave emission may occur in different regions on the Bloch sphere, possibly leading to different non-equilibrium phases.

IV. CONCLUSIONS

In conclusion, in this work we have studied the the post-quench dynamics of a fully-connected p -spin model ($p > 2$) perturbed by a short-ranged interaction, controlled by the coupling J , generalizing to arbitrary values of p the system studied in previous work [26, 32, 34]. In the mean-field limit of $J = 0$, the dynamics is equivalent to the one of a particle in a classical energy landscape: a DPT emerges, driven by the transverse field g , whose order depends on the parity of p , for $p > 2$, which determines the qualitative shape of the effective potential. In particular, we find a second order dynamical transition for odd p (where the potential is an asymmetric double-well) and first order one for even p (where the profile is made by three basins). The nature of this transition is modified by the presence of a short-range perturbation, treated in the

framework of the non-equilibrium spin-wave theory. The latter generates an effective damping in the dynamics which is maximal in a region close to the paramagnetic North pole: this changes the nature of the dynamical phases -now being defined by the behaviour of the magnetization in a prethermal regime- that appear on the phase diagram, where the short-range coupling drives a new first-order transition for $p \geq 3$ odd, while displaying a subtle transition for $p \geq 4$ even, detected in the order parameter fluctuations and being of the first-order like the one obtained in the mean-field limit.

In fact, the analysis discussed here can be straightforwardly generalized to a wider class of fully-connected spin models with generic integrability breaking terms: the profile of the energy landscape and the direction where interaction induced by the integrability breaking perturbation is oriented are the only two ingredients which fully determine the features of the non-equilibrium phase diagram.

Acknowledgements — We thank A. Lerose and S. Pappalardi for interesting discussions and useful comments on the manuscript.

Appendix A: The effective energy landscape

In this section we discuss in greater detail the properties of the effective potential $\mathcal{H}_{cl}(\vec{S}, g) = -\lambda(S^x)^p - gS^z$, determining the dynamics of the magnetization $\vec{S} = \sum_i \vec{\sigma}_i/N$ in the thermodynamic limit, $N \rightarrow \infty$. In particular, we aim to characterize the stationary points of the potential for $g > 0$ and in the Northern hemisphere ($S^z > 0$) of the Bloch sphere, where the dynamics takes place for the protocol described in the main text (as shown in Fig. 2-(a) and (d) of the main text). Parameterizing the magnetization with polar angles $(\theta, \phi) \in [0, \pi/2] \times [0, 2\pi]$, as $\vec{S} = (\sin \theta \cos \phi, \sin \theta \sin \phi, \cos \theta)$, the equations for the stationary points of \mathcal{H}_{cl} are:

$$\begin{cases} \frac{\partial \mathcal{H}_{cl}}{\partial \phi} = -\lambda p (\sin \theta)^p (\cos \phi)^{p-1} \sin \phi = 0 \\ \frac{\partial \mathcal{H}_{cl}}{\partial \theta} = -\lambda p (\sin \theta)^{p-1} (\cos \phi)^p \cos \theta + g \sin \theta = 0 \end{cases} \quad (\text{A1})$$

One possible solution is given by $\theta = 0$ and ϕ undetermined (the North Pole of the Bloch sphere), being a maximum for $p = 2$ and a minimum for $p > 2$. All the other solutions are obtained by solving the system:

$$\begin{cases} \sin \phi = 0 \\ (\sin \theta)^{p-2} \cos \theta (\cos \phi)^p = \frac{g}{\lambda p} \end{cases} \quad (\text{A2})$$

The first equation, solved by $\phi = 0$ or π , tells us that the stationary points lie in the plane $S^y = 0$. If we focus on the case of $\phi = 0$, then θ solves from the equation

$$(\sin \theta)^{p-2} \cos \theta = \frac{g}{\lambda p} \quad (\text{A3})$$

For sufficiently low values g , the equation (A3) admits either one solution for $p = 2$, corresponding to a single minimum, or one local maximum and one local minimum for $p > 2$. For p even, the same solution(s) for θ can be associated also to $\phi = \pi$, while for p odd there is no solution for $\phi = \pi$. As a result, the profile of the effective potential $\mathcal{H}_{cl}(\vec{S}, g)$ is either a double well, for $p = 2$ or $p \geq 3$ odd, or a triple well for $p \geq 4$ even, as shown in Fig. 1 of

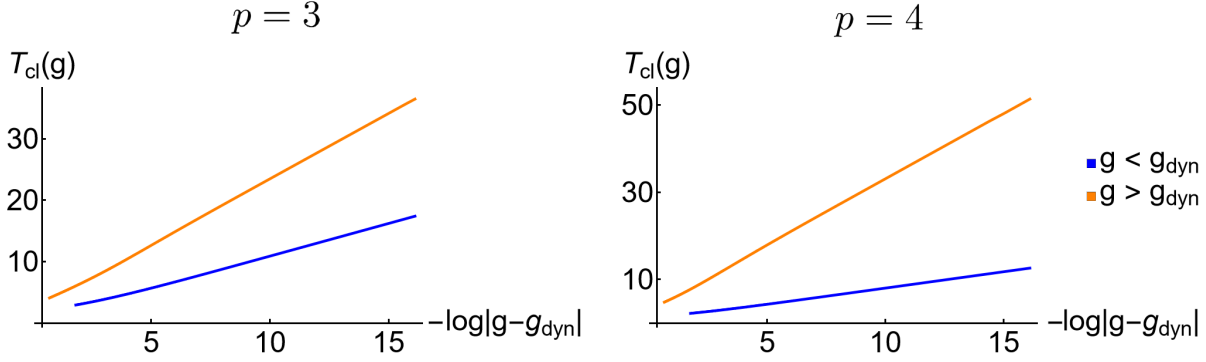


FIG. 7. Plot of the period $T_{cl}(g)$ of the classical trajectories originating from the dynamics discussed in Sec. II of the main text, respectively for $p = 3$ (left) and $p = 4$ (right). $T_{cl}(g)$ is compared against $\log|g - g_{dyn}|$, both for $g < g_{dyn}$ (blue) and $g > g_{dyn}$ (orange). We pose $\lambda = 1$, like in the main text.

the main text. The existence of such stationary points is not guaranteed for large values of g . More precisely, it can be shown that at $g = g_{sp} = p(p-2)^{(p-2)/2}/(p-1)^{(p-1)/2}$, the local maximum and the local minimum coalesce into a single inflection point and that for $g > g_{sp}$ the profile becomes a single well, having only one minimum at $\vec{S} = \hat{z}$ ($\theta = 0$). The value g_{sp} of the transverse field where this change occurs is called spinodal point [44].

The topology of the potential profile, defined in terms of its stationary points, also affects the post quench dynamics starting from $S^x(0) = 1$ explored in the main text. In particular the mean-field dynamical transition, occurs at the point $g = g_{dyn}$ where the energy of the initial configuration matches the one of the local maximum \vec{S}_c . This can be found by numerically solving equation (A3), together with

$$-\lambda(\sin \theta)^p - g \cos \theta = -g, \quad (\text{A4})$$

which stands for $\mathcal{H}_{cl}(\vec{S}(0)) = \mathcal{H}_{cl}(\vec{S}_c)$.

It can be easily checked that $g_{sp} > g_{dyn}$, for any $p \geq 2$. Indeed, fixing $g = g_{sp}$ and either $\phi = 0$ or $\phi = \pi$, \mathcal{H}_{cl} is a monotonically increasing function of θ (as it is single-well shaped at $g = g_{sp}$). This means that the energy of the initial condition $\vec{S}(0) = \hat{x}$ (i.e. $\theta = \pi/2$, $\phi = 0$) is strictly greater than the one of the coalesced stationary point (retrieved at $\theta < \pi < 2$, as one can check from eq.(A3)), for any p . By continuity we also get that that the energy of $\vec{S}(0)$ is greater than the one of the maximum for g slightly below g_{sp} , so that by definition $g_{sp} > g_{dyn}$. The last inequality implies that the effective potential displays multiple wells at the mean-field dynamical transition, justifying the connection between the dynamical criticality and the topology of the landscape, that has been made in the main text. The multi-well shape of $\mathcal{H}_{cl}(\vec{S})$ also implies that its local maxima have a non-vanishing θ , a feature which is crucial to determine the order of the dynamical transition for $p \geq 4$ even (see also Appendix B).

Appendix B: The period of classical orbits and its relation with dynamical singularities

In this appendix we derive a closed formula for the period $T_{cl}(g)$ of the classical orbits discussed in Sec. II of the main text. In particular, we show that $T_{cl}(g)$ diverges logarithmically when approaching the transition point $g = g_{dyn}$ both from above and below and discuss how show that such a singularity is retrieved also in $\overline{S^x}(g)$.

To compute $T_{cl}(g)$ do so, we first perform the change of variables:

$$S^x = Q, \quad S^y = \sqrt{1 - Q^2} \cos(2P), \quad S^z = \sqrt{1 - Q^2} \sin(2P) \quad (\text{B1})$$

where $Q \in [-1, 1]$ and $P \in [0, \pi]$. By doing so, it can be shown [32, 44] that the dynamics described by the equations (2) is an Hamilton dynamics induced by the effective Hamiltonian

$$\mathcal{H}_{cl}(Q, P) = -\frac{\lambda}{2} Q^p - g \sqrt{1 - Q^2} \sin(2P) \quad (\text{B2})$$

The first of the Hamilton equations is

$$\partial_t Q = -2g \sqrt{1 - Q^2} \cos(2P) \quad (\text{B3})$$

Plugging eq. (B3) into the expression (B2), one straightforwardly obtains the following expression:

$$(2\mathcal{H}_{cl}(Q, P) + \lambda Q^p)^2 = 4g^2(1 - Q^2) - (\partial_t Q)^2 \quad (\text{B4})$$

Then, if we fix the initial energy $\mathcal{H}_{cl}(Q(0), P(0)) = E_0$, we can solve the dynamics by separation of variables to obtain

$$t = \int_{\min(Q(0), Q(t))}^{\max(Q(0), Q(t))} \frac{dx}{\sqrt{4g^2(1 - x^2) - (2E_0 + \lambda x)^p}} \quad (\text{B5})$$

This formula gives us the period of the classical orbits studied in the main text, if we fix the initial condition $\vec{S}(0) = \hat{x}$ (i.e. $Q(0) = 1$, $P(0) = 0$ and $E_0 = -\lambda$), arriving at

$$T_{cl}(g) = 2 \int_{q_1}^1 \frac{dx}{\sqrt{4g^2(1 - x^2) - (\lambda x - 2\lambda)^p}} \quad (\text{B6})$$

where q_1 is the turning point of the orbit, obtained as the solution of the equation $\mathcal{H}_{cl}(Q, P = 0) = \mathcal{H}_{cl}(Q = 1, P = 0) = -\lambda$ (for $Q \neq 1$). We compute $T_{cl}(g)$ numerically from eq. (B6), for several values of g and for the paradigmatic cases of $p = 3$ and $p = 4$. The result, shown in Fig. 7, is that for $g \rightarrow g_{dyn}^\pm$ the period diverges as $T_{cl} \sim \log |g - g_{dyn}|^{-1}$, with a prefactor which is different above and below g_{dyn} .

The divergence of $T_{cl}(g)$ at g_{dyn} is connected to change of topology of the underlying trajectories, being confined in a single ferromagnetic well for $g < g_{dyn}$ and exploring the whole landscape for $g > g_{dyn}$. In particular, at $g = g_{dyn}$ the trajectory is a *separatrix*, that is a singular, non-periodic orbit where any dynamics converges, for late times, to the nearest local maximum S_c^x , separating the well where the motion takes place from the others. For any value of p , this implies that $\overline{S^x}(g_{dyn}) = S_c^x$. $T_{cl}(g)$ can be also connected to the type of singularity displayed by $\overline{S^x}$, when approaching the transition point from below: as $g \rightarrow g_{dyn}^-$, the orbits evolving into the rightmost ferromagnetic well develop a plateau of diverging length near S_c^x (see Fig. 2-(c) and (f) of the main text), so that $\overline{S^x}$ can be qualitatively estimated as

$$\overline{S^x}(g) = \frac{1}{T_{cl}(g)} \int_0^{T_{cl}(g)} dt S^x(t) = S_c^x + \frac{1}{T_{cl}(g)} \int_0^{T_{cl}(g)} dt (S^x(t) - S_c^x) \simeq S_c^x + \frac{c}{T_{cl}(g)}, \quad (\text{B7})$$

if we assume that the integral $\int_0^{T_{cl}(g)} dt (S^x(t) - S_c^x)$ is bounded and converges to a positive constant $c > 0$ at the transition point. The estimate in eq. (B7) implies that $\overline{S^x} - S_c^x \propto 1/\log(g_{dyn} - g)^{-1}$ approaching the transition from below: such a log-singularity is quantitatively confirmed by the results shown in Fig. 8, obtained by computing $\overline{S^x}$ numerically (as in Sec.II of the main text) and S_c^x from the eq. (A3) and (A4) (as discussed in Appendix A).

While the singularities in the time-average magnetization $\overline{S^x}$ are intimately connected to the one of the periods, its continuity is determined by the topology of the effective potential, as discussed in the main text, thus by the value of p . In particular:

- For $p \geq 3$ odd, the dynamics for $g \rightarrow g_{dyn}^+$ $\overline{S^x}$ develops a plateau at the *only* local maximum of the landscape S_c^x (see Fig.2-(c) of the main text), so that $\lim_{g \rightarrow g_{dyn}^+} \overline{S^x} = S_c^x$ and the transition is continuous in this case.
- For $p \geq 4$ even, $\overline{S^x} = 0$ for any $g > g_{dyn}$, due to the symmetry of the orbits, so that $\overline{S^x}$ is discontinuous at the transition. In particular, the plot in Fig.2-(f) of the main text shows that the magnetization spends an equal, diverging amount of time near close to each of the two local maxima at S_c^x and $-S_c^x$. At the origin of the discontinuity lies thus the non-symmetric role played by the opposite ferromagnetic maximum at $-S_c^x$, respectively above and below the transition point.

Appendix C: Review of non-equilibrium spin-wave analysis

In this appendix, we review the time-dependent spin-wave analysis, following Ref. [34]. This is implemented essentially in three steps:

1. first, we express the dynamical evolution in a rotating reference frame \mathcal{R} , defined in such a way that the magnetization is always aligned with the \mathbf{Z} -axis;
2. performing an Holstein-Primakoff in \mathcal{R} , we introduce the *spin-waves*, defined as canonical coordinates representing the spatial fluctuation of the collective spin on various length scales;
3. we derive a set of coupled equations describing the evolution of the collective spin, which is obtained requiring that that the frame \mathcal{R} is aligned with the collective spin at any time, and of the spin-wave correlators, which act as a quantum feedback on the former.

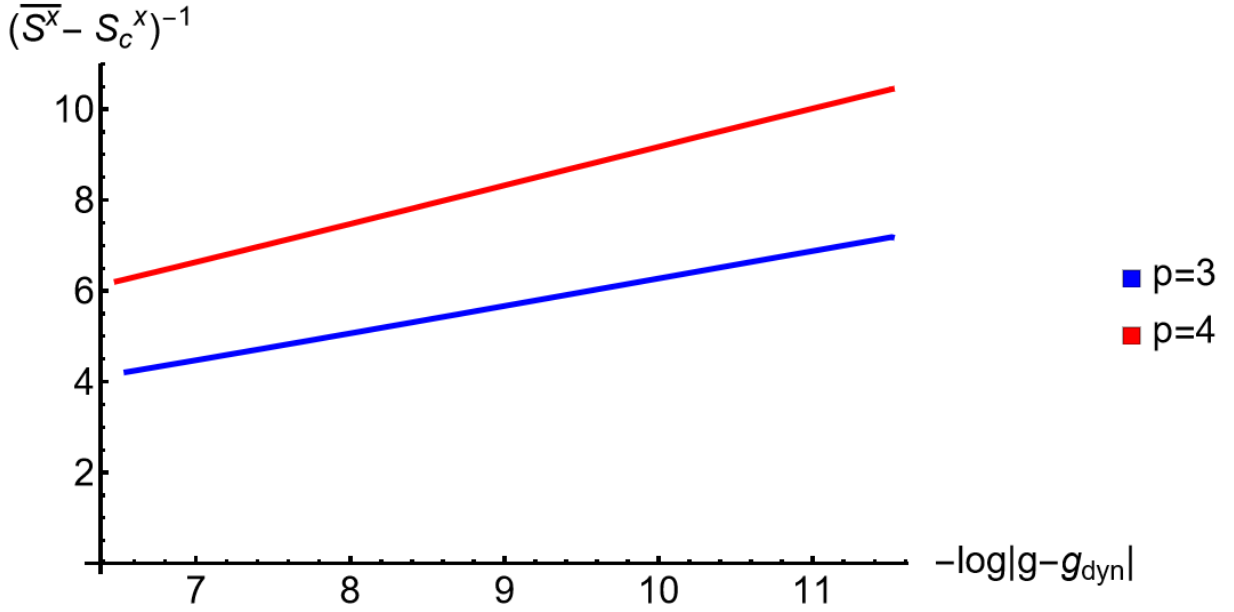


FIG. 8. Plot of the singularity of the time-average magnetization $\overline{S^x}$, for the trajectories originating from the dynamics discussed in Sec. II of the main text, respectively for $p = 3$ (blue) and $p = 4$ (red). $\overline{S^x}$ is plotted as a function of g in the dynamical ferromagnetic phase, where $g < g_{dyn}$, and S_c^x is defined as an unstable stationary point of the potential in eq.(3) of the main text at g_{dyn} .

1. Rotating frame of reference coordinates

We approach the problem by rewriting down the full Hamiltonian in a time-dependent, rotating frame of reference, generalizing our calculations to generic spin s . Assuming periodic boundary conditions, the Hamiltonian can be written as

$$\hat{H} = -\frac{\lambda}{N^{p-1}} (\tilde{\sigma}_0^x)^p - g\tilde{\sigma}_0^z - \frac{J}{N} \sum_{k \neq 0} \cos k \tilde{\sigma}_k^x \tilde{\sigma}_{-k}^x, \quad (\text{C1})$$

where the Fourier modes are defined as $\tilde{\sigma}_k^\alpha = \sum_{j=1}^N e^{-ikj} \sigma_j^\alpha$ (with $\sigma_j^\alpha = \hat{s}_j^\alpha/s$ being the rescaled spin operator on the lattice site j) and $k = 2\pi n/N$ for $n = 0, \dots, N-1$, N being the system size.

The Hamiltonian can be also split into a mean-field term $\hat{H}_0 = \lambda(\tilde{\sigma}_0^x)^p/N^{p-1} - g\tilde{\sigma}_0^z$, depending on the collective spin only, and a short-range perturbation $\hat{U} = -J \sum_{k \neq 0} \cos k \tilde{\sigma}_k^x \tilde{\sigma}_{-k}^x/N$, as done in the main text.

The reference frame \mathcal{R} is identified by the time-dependent Cartesian vector basis $\{\mathbf{X}(t), \mathbf{Y}(t), \mathbf{Z}(t)\}$, whose components in the original frame $\{\mathbf{x}, \mathbf{y}, \mathbf{z}\}$ read as

$$\mathbf{X} = \begin{pmatrix} \cos \theta(t) \cos \phi(t) \\ \cos \theta(t) \sin \phi(t) \\ -\sin \theta(t) \end{pmatrix}; \quad \mathbf{Y} = \begin{pmatrix} -\sin \phi(t) \\ \cos \phi(t) \\ 0 \end{pmatrix}; \quad \mathbf{Z} = \begin{pmatrix} \sin \theta \cos \phi(t) \\ \sin \theta \sin \phi(t) \\ \cos \theta(t) \end{pmatrix}$$

and where the spherical angles $\theta(t)$ and $\phi(t)$ are defined so that the average magnetization $\vec{S}(t) = \langle \sum_j \vec{\sigma}_j(t) \rangle / N$ is always aligned with $\mathbf{Z}(t)$. This change of frame is implemented on the spin Hilbert space by the time-dependent unitary rotation

$$V(\theta(t), \phi(t)) = \exp(-is\phi(t) \sum_i \sigma_i^z) \exp(-is\theta(t) \sum_i \sigma_i^y)$$

so that the spin operators transform accordingly :

$$V\sigma_j^x V^\dagger = \mathbf{X} \cdot \vec{\sigma}_j \equiv \sigma_j^X, \quad V\sigma_j^y V^\dagger = \mathbf{Y} \cdot \vec{\sigma}_j \equiv \sigma_j^Y, \quad V\sigma_j^z V^\dagger = \mathbf{Z} \cdot \vec{\sigma}_j \equiv \sigma_j^Z, \quad (\text{C2})$$

In this new frame, the Heisenberg equation of motion can be written as

$$\frac{d}{dt} \sigma_j^\alpha = -i[\sigma_j^\alpha, \tilde{H}] \quad (\text{C3})$$

where the modified Hamiltonian

$$\tilde{H} = H + iV\dot{V}^\dagger \quad (\text{C4})$$

includes an additional term $iV\dot{V}^\dagger = -s\vec{\omega}(t) \cdot \sum_j \vec{\sigma}_j$, where $\vec{\omega}(t) = (-\sin\theta\dot{\phi}, -\dot{\theta}, \cos\theta\dot{\phi})$, playing the same role of apparent forces in classical mechanics. In the rotating frame \mathcal{R} , \tilde{H} has the following form:

$$\begin{aligned} \frac{\tilde{H}}{N} = & -g \left[(\mathbf{X} \cdot \mathbf{z}) \frac{\tilde{\sigma}_0^X}{N} + (\mathbf{Y} \cdot \mathbf{z}) \frac{\tilde{\sigma}_0^Y}{N} + (\mathbf{Z} \cdot \mathbf{z}) \frac{\tilde{\sigma}_0^Z}{N} \right] - \lambda \left[(\mathbf{X} \cdot \mathbf{x}) \frac{\tilde{\sigma}_0^X}{N} + (\mathbf{Y} \cdot \mathbf{x}) \frac{\tilde{\sigma}_0^Y}{N} + (\mathbf{Z} \cdot \mathbf{x}) \frac{\tilde{\sigma}_0^Z}{N} \right]^p \\ & - J \sum_{k \neq 0} \cos k \left[(\mathbf{X} \cdot \mathbf{x}) \frac{\tilde{\sigma}_k^X}{N} + (\mathbf{Y} \cdot \mathbf{x}) \frac{\tilde{\sigma}_k^Y}{N} + (\mathbf{Z} \cdot \mathbf{x}) \frac{\tilde{\sigma}_k^Z}{N} \right] \left[(\mathbf{X} \cdot \mathbf{x}) \frac{\tilde{\sigma}_{-k}^X}{N} + (\mathbf{Y} \cdot \mathbf{x}) \frac{\tilde{\sigma}_{-k}^Y}{N} + (\mathbf{Z} \cdot \mathbf{x}) \frac{\tilde{\sigma}_{-k}^Z}{N} \right] \\ & + \sin\theta s\dot{\phi} \frac{\tilde{\sigma}_0^X}{N} - s\dot{\theta} \frac{\tilde{\sigma}_0^Y}{N} - \cos\theta s\dot{\phi} \frac{\tilde{\sigma}_0^Z}{N}, \end{aligned} \quad (\text{C5})$$

Once the equations of motion are formally written in the new frame, $\theta(t)$ and $\phi(t)$ are obtained self-consistently by imposing that

$$\begin{cases} \langle \tilde{\sigma}_0^X(t) \rangle = 0 \\ \langle \tilde{\sigma}_0^Y(t) \rangle = 0 \end{cases} \quad (\text{C6})$$

2. Holstein-Primakoff transformation

The main idea at the basis of time-dependent spin-wave theory is that in the new frame, as long as the spatial fluctuations induced by the short-range coupling J are weak enough, these act as a small perturbation on top of a "classical" average collective spin. In this case, we can rewrite the spin operators via the well known Holstein-Primakoff transformation [55]

$$\begin{cases} \sigma_j^X \sim q_j/\sqrt{s} + O(1/s^{3/2}) \\ \sigma_j^Y \sim p_j/\sqrt{s} + O(1/s^{3/2}) \\ \sigma_j^Z = 1 - \frac{q_j^2 + p_j^2 - 1}{2s} \end{cases} \quad (\text{C7})$$

expanded in powers of $1/\sqrt{s}$ and truncated to the leading order. In terms of the Fourier space variables $\tilde{q}_k = \sum_r e^{-ikr} q_r/\sqrt{N}$ and $\tilde{p}_k = \sum_r e^{-ikr} p_r/\sqrt{N}$, can also be expressed as [55]:

$$\begin{cases} \frac{\tilde{\sigma}_k^X}{N} \sim \tilde{q}_k/\sqrt{Ns} + O(1/s^{3/2}) \\ \frac{\tilde{\sigma}_k^Y}{N} \sim \tilde{p}_k/\sqrt{Ns} + O(1/s^{3/2}) \\ \frac{\tilde{\sigma}_k^Z}{N} = 1 - \frac{1}{2Ns} \sum_{k'} (\tilde{q}_{k'}\tilde{q}_{k-k'} + \tilde{p}_{k'}\tilde{p}_{k-k'} - \delta_{k,0}) \end{cases} \quad (\text{C8})$$

This approximation is exact both in the limit of large spin $s \rightarrow \infty$, or, as stated before, when the spin-wave degree of excitation is kept small throughout the dynamics, in a sense which is made clear below.

The whole sense of our approximation is that we are expanding on-site fluctuations of the spin along the \mathbf{Z} -axis in terms of harmonic excitations, defined in terms of ladder operators $\hat{a}_j = (q_j + ip_j)/\sqrt{2}$ and his conjugate \hat{a}_j^\dagger : their Fourier Transform $\tilde{a}_k = \sum_j e^{-ikj} \hat{a}_j/\sqrt{N}$ represent the spin-wave excitations which destroy coherence in the system, causing a depletion of the magnetization length, which can be rewritten as $|\langle \tilde{\sigma}_0^Z(t) \rangle/N| = 1 - \epsilon(t)$, where

$$\epsilon(t) \equiv \frac{1}{Ns} \sum_{k \neq 0} \langle \tilde{a}_k^\dagger \tilde{a}_k(t) \rangle = \frac{1}{Ns} \sum_{k \neq 0} \left\langle \frac{\tilde{q}_k(t)\tilde{q}_{-k}(t) + \tilde{p}_k(t)\tilde{p}_{-k}(t) - 1}{2} \right\rangle \quad (\text{C9})$$

is the spin-wave density. Thus, the the time-dependent spin-wave theory is valid as long as $\epsilon(t) \ll 1$.

3. Equations of motion for weak spin-wave excitation

As long as the spin-wave excitation density $\epsilon(t)$ is small, it is reasonable to assume that the dynamics is dominated by terms of lowest nontrivial order in the operators $\{(\tilde{q}_k, \tilde{p}_k)\}$ (from eq. (C8)), that is by a Gaussian approximation,

in our case. Exactly as in the case of Ref. [34], an expansion of the Hamiltonian in eq.(C5), this amounts to keeping the terms

$$\begin{aligned} \hat{U}_1 = & \frac{\tilde{q}_0}{\sqrt{N_s}} \left\{ s \sin \theta \dot{\phi} - p\lambda(\mathbf{Z} \cdot \mathbf{x})^{p-1}(\mathbf{X} \cdot \mathbf{x}) \left(1 - (p-1) \frac{\hat{n}_{SW}}{N_s} \right) - g(\mathbf{X} \cdot \mathbf{z}) + \right. \\ & \left. + \frac{2(\mathbf{Z} \cdot \mathbf{x})}{N_s} \sum_{k \neq 0} J \cos k [(\mathbf{X} \cdot \mathbf{x}) \tilde{q}_k \tilde{q}_{-k} + (\mathbf{Y} \cdot \mathbf{x}) \frac{\tilde{q}_k \tilde{p}_{-k} + \tilde{p}_k \tilde{q}_{-k}}{2}] \right\} + \end{aligned} \quad (C10)$$

$$\begin{aligned} & + \frac{\tilde{p}_0}{\sqrt{N_s}} \left\{ -s\dot{\theta} - p\lambda(\mathbf{Z} \cdot \mathbf{x})^{p-1}(\mathbf{Y} \cdot \mathbf{x}) \left(1 - (p-1) \frac{\hat{n}_{SW}}{N_s} \right) - g(\mathbf{Y} \cdot \mathbf{z}) + \right. \\ & \left. + \frac{2(\mathbf{Z} \cdot \mathbf{x})}{N_s} \sum_{k \neq 0} J \cos k [(\mathbf{Y} \cdot \mathbf{x}) \tilde{p}_k \tilde{p}_{-k} + (\mathbf{X} \cdot \mathbf{x}) \frac{\tilde{q}_k \tilde{p}_{-k} + \tilde{p}_k \tilde{q}_{-k}}{2}] \right\} \end{aligned}$$

$$\hat{U}_2^{(0)} = (p\lambda(\mathbf{Z} \cdot \mathbf{x})^p + g(\mathbf{Z} \cdot \mathbf{z}) + s \cos \theta \dot{\phi}) \frac{1}{N_s} \sum_{k \neq 0} \hat{n}_k \quad (C11)$$

$$\hat{U}_2 = -\frac{1}{N_s} \sum_{k \neq 0} J \cos k \{ (\mathbf{X} \cdot \mathbf{x})^2 \tilde{q}_k \tilde{q}_{-k} + (\mathbf{Y} \cdot \mathbf{x})^2 \tilde{p}_k \tilde{p}_{-k} + 2(\mathbf{X} \cdot \mathbf{x})(\mathbf{Y} \cdot \mathbf{x}) \frac{\tilde{q}_k \tilde{p}_{-k} + \tilde{p}_k \tilde{q}_{-k}}{2} \} \quad (C12)$$

In particular, the terms $\hat{U}_2^{(0)}$ and \hat{U}_2 represent the quadratic part from the expansion of the mean-field term \hat{H}_0 and the short-range perturbation \hat{U} , respectively. Within such approximation, the dynamics of the time-dependent frame \mathcal{R} is determined imposing the conditions (C6), leading to

$$\begin{cases} s\dot{\phi} = p\lambda(\sin \theta)^{p-2}(\cos \phi)^p \cos \theta \{ 1 - (p-1)\epsilon(t) \} - g - 2J\delta^{qq}(t) \cos \theta \cos^2 \phi + 2J\delta^{qp}(t) \sin \phi \cos \phi \\ s\dot{\theta} = p\lambda(\sin \theta \cos \phi)^{p-1} \sin \phi \{ 1 - (p-1)\epsilon(t) \} - 2J\delta^{pp}(t) \sin \theta \sin \phi \cos \phi + 2J\delta^{qp}(t) \sin \theta \cos \theta \cos^2 \phi \end{cases} \quad (C13)$$

with the quantum feedback being $\delta^{\alpha\beta}(t) \equiv \sum_{k \neq 0} \Delta_k^{\alpha\beta} \cos k / (N_s)$ for $\alpha, \beta \in \{p, q\}$, as stated in the main text (the correlators $\Delta_k^{\alpha\beta}$ are defined also below).

We see that, within time-dependent spin-wave theory, the motion of the collective spin is coupled to the one of the correlation functions

$$\Delta_k^{qq}(t) = \langle \tilde{q}_{-k}(t) \tilde{q}_k(t) \rangle, \quad \Delta_k^{qp}(t) = \left\langle \frac{\tilde{q}_{-k}(t) \tilde{p}_k(t) + \tilde{p}_{-k}(t) \tilde{q}_k(t)}{2} \right\rangle, \quad \Delta_k^{pp}(t) = \langle \tilde{p}_{-k}(t) \tilde{p}_k(t) \rangle \quad (C14)$$

defined for $k \neq 0$, where all the averages are performed with respect to the initial state. The evolution of the variables $\{\Delta_k^{\alpha\beta}(t)\}$ is straightforwardly determined by the Heisenberg equations of motion for the canonical variables $(\tilde{q}_k, \tilde{p}_k)$:

$$\begin{cases} s \frac{d\tilde{q}_k}{dt} = (p\lambda(\sin \theta)^{p-2}(\cos \phi)^p - 2J \cos k \sin^2 \phi) \tilde{p}_k + 2J \cos k \cos \theta \sin \phi \cos \phi \tilde{q}_k \\ s \frac{d\tilde{p}_k}{dt} = -(\lambda(\sin \theta)^{p-2}(\cos \phi)^p - 2J \cos k \cos^2 \phi \cos^2 \theta) \tilde{q}_k - (2J \cos k \cos \theta \sin \phi \cos \phi) \tilde{p}_k \end{cases} \quad (C15)$$

and reads as

$$\begin{cases} s \frac{d}{dt} \Delta_k^{qq} = (4J \cos k \cos \theta \sin \phi \cos \phi) \Delta_k^{qq} + \{ 2p\lambda(\sin \theta)^{p-2}(\cos \phi)^p - 4J \cos k \sin^2 \phi \} \Delta_k^{qp} \\ s \frac{d}{dt} \Delta_k^{qp} = -\{ p\lambda(\sin \theta)^{p-2}(\cos \phi)^p - 2J \cos k \cos^2 \phi \cos^2 \theta \} \Delta_k^{qq} \\ \quad + \{ p\lambda(\sin \theta)^{p-2}(\cos \phi)^p - 2J \cos k \sin^2 \phi \} \Delta_k^{pp} \\ s \frac{d}{dt} \Delta_k^{pp} = -\{ 2p\lambda(\sin \theta)^{p-2}(\cos \phi)^p - 4J \cos k \cos^2 \phi \cos^2 \theta \} \Delta_k^{qp} \\ \quad - (4J \cos k \cos \theta \sin \phi \cos \phi) \Delta_k^{pp} \end{cases} \quad (C16)$$

From equations Eq.(C16), it is also possible to prove that, for any fixed momentum k , the time-evolution of the three spin-wave correlators is completely specified by two of them, as they have to satisfy the constraint

$$(\Delta_k^{qp}(t))^2 = \Delta_k^{qq}(t) \Delta_k^{pp}(t) - \frac{1}{4}. \quad (C17)$$

at any time t . The final result is that, within the framework of time-dependent spin-wave theory, the dynamics of the average magnetization $\langle \vec{S}(t) \rangle$ is coupled with that of the spin-wave correlation functions $\Delta^{\alpha\beta}(t)$, which also determine the spin-wave density (see eq.(C9))

$$\epsilon(t) = \frac{1}{Ns} \sum_{k \neq 0} \frac{\Delta_k^{qq}(t) + \Delta_k^{pp}(t) - 1}{2}. \quad (\text{C18})$$

Integrating simultaneously the system of equations (C13) and (C16) and checking that $\epsilon(t) \ll 1$, one obtains the non-equilibrium dynamics of $\langle \vec{S}(t) \rangle$, coupled to spin-wave fluctuations. The initial conditions are determined by the initial state $|\psi_0\rangle$. The case we studied is the one of a quench in the Hamiltonian (C1), with pre-quenches values given by $g = g_0$ and $J = 0$, which correspond to

$$\begin{aligned} \{\sin \theta(t=0)\}^{p-2} \cos \theta(t=0) &= g_0/(\lambda p), \quad \phi(t=0) = 0, \\ \Delta_k^{qq}(t=0) = \Delta_k^{pp}(t=0) &= 1/2, \quad \text{and} \quad \Delta_k^{qp}(t=0) = 0, \end{aligned} \quad (\text{C19})$$

for every $k \neq 0$. This also imply that $\epsilon(t=0) = 0$, as the initial ground state $|\psi_0\rangle = |\rightarrow \cdots \rightarrow\rangle$ is perfectly coherent, with the spin on each lattice site point in the direction of the ferromagnetic minimum of \hat{H} . From the first and the second of eq. (C16), we can also get an evolution equation for $\epsilon(t)$, written as

$$\frac{d\epsilon(t)}{dt} = 4 \frac{J}{s} \cos \theta \sin \phi \cos \phi \delta^{qq}(t) + 4 \frac{J}{s} (\cos^2 \theta \cos^2 \phi - \sin^2 \phi) \delta^{qp}(t). \quad (\text{C20})$$

The spin-wave emission rate, $d\epsilon/dt$, is then governed by the couplings $C_1(\theta, \phi) = \cos \theta \sin \phi$ and $C_2(\theta, \phi) = \cos^2 \theta \cos^2 \phi - \sin^2 \phi$ which, by construction, are derived from the quadratic expansion \hat{U}_2 (see eq. (C12)) of the short term perturbation \hat{U} (see (6) of the main text), projected on the rotating frame \mathcal{R} , while being completely independent of \hat{H}_0 . Changing the direction of the short-ranged interaction, the $C_1(\theta, \phi)$ and $C_2(\theta, \phi)$ are modified as the dependence of \hat{U}_2 on θ and ϕ is.

In the fully-connected limit $J \rightarrow 0$ the evolution of the collective spin decouples from the fluctuations, and the equations (C13) are identical to the ones predicted by the effective classical theory described in Ref. [32]. In this case, the spin-wave correlators still have nontrivial dynamics, but the spin-wave density is conserved and always vanishes.

Appendix D: Details on the first-order transition line

In this appendix, examine in greater detail the discontinuity line $J = J_{dyn}(g)$, appearing in Fig. 3 (left) and Fig.4 (right) of the main text, analyzing the cases of $p = 3$ and $p = 4$ separately.

For $p = 3$, the transition line $J_{dyn}(g)$ emerges clearly fixing a sufficiently large value of g : the plot in Fig. 9 (top-right) shows that the time-average magnetization \bar{S}^x has a discontinuity in J , though not being either completely smooth J above and below the discontinuity point, because of the noise induced by the spin-wave emission. In this regime, it is possible to make a semi-analytical estimation of the point $J_{dyn}(g)$ where the transition happens, as discussed in the following. First we notice that, because of the squeezing of the potential, due to the spin-wave excitation and expressed by the eq.(16) of the main text, the dynamics is driven by an effective transverse field

$$g_\epsilon = \frac{g}{(1 - \epsilon)^{p-1}} \quad (\text{D1})$$

which depends on time through ϵ . Thus, for any fixed g it exists a threshold value ϵ_{sp} , set by the equation[61].

$$\frac{g}{(1 - \epsilon)^{p-1}} = g_{sp} \quad (\text{D2})$$

such that whenever $\epsilon > \epsilon_{sp}$, the squeezed potential in eq.(16) displays a single paramagnetic well. An intuitive, *sufficient* condition for the localization of the magnetization in the paramagnetic well can be set by the statement that $\epsilon(t)$ is asymptotically greater ϵ_{sp} for large times, that is

$$\bar{\epsilon} = \lim_{T \rightarrow \infty} \frac{1}{T} \int_0^T \epsilon(t) dt > \epsilon_{sp} \quad (\text{D3})$$

This condition implies that, for large times, the squeezed potential from eq.(16) displays a single, paramagnetic well, where the magnetization is by definition localized. The plots in Fig.9 (left) show that, fixing a sufficiently large g , the

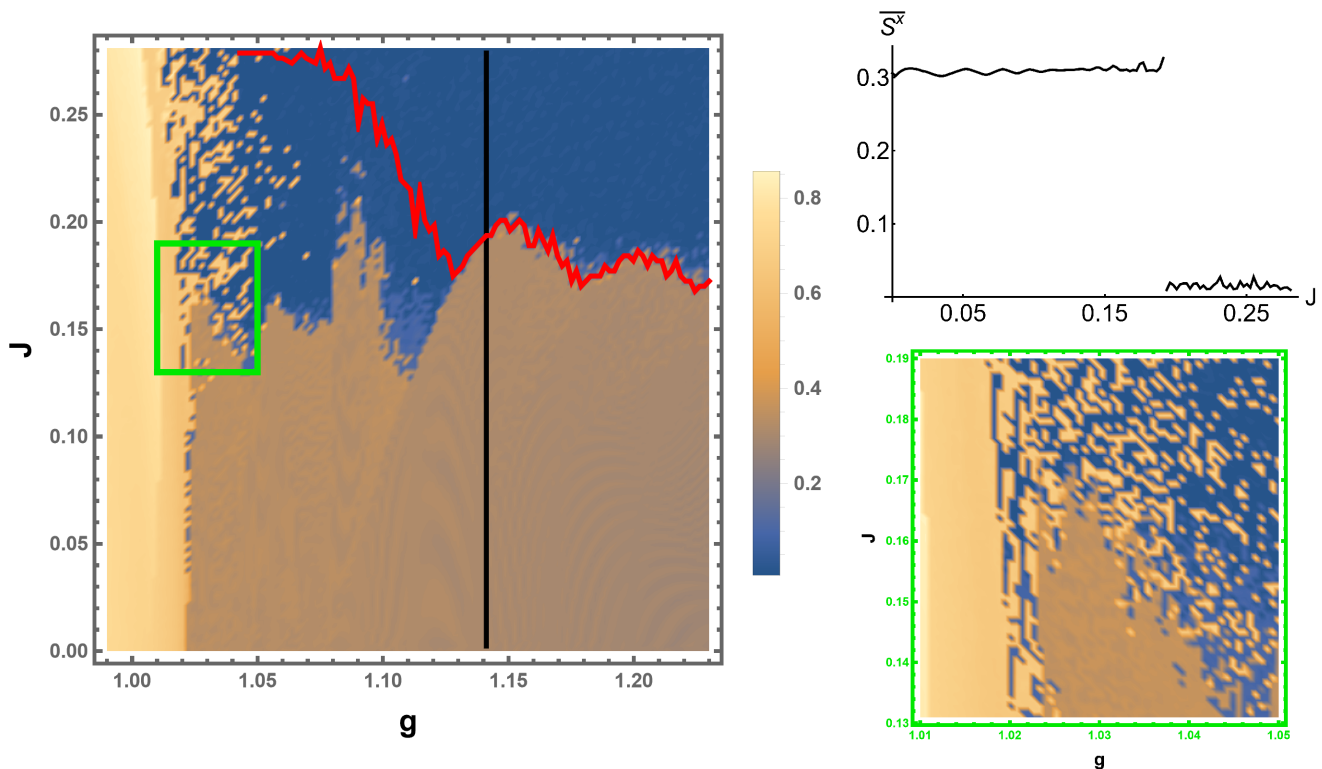


FIG. 9. (Color online) Non-equilibrium phase diagram for the p -spin model in eq. (1), for $p = 3$. **(Left)** Over the same phase diagram shown in Fig. 3 (left) of the main text, we plot the threshold line (red), above which $\bar{\epsilon} > \epsilon_{sp}$ (see details in Appendix D). The black vertical line and the green box indicate the values of g and J investigated in the plots on the right. **(Top-right)** Plot of the time-averaged magnetization \bar{S}^x , as function of J and at fixed $g \simeq 1.142$ (black line on the phase diagram on the left). \bar{S}^x is discontinuous around $J \simeq 0.194$. **(Bottom-right)** Inset from the phase diagram on the left (in the green box), around the chaotic region where the second-order and first-order transition line merge.

values of J where $\bar{\epsilon}$ overcomes the threshold ϵ_{sp} matches the transition point $J_{dyn}(g)$: this provides a semi-analytical argument for the prediction of $J_{dyn}(g)$ at large g , as the threshold ϵ_{sp} can be predicted analytically, but there is no explicit formula relating $J_{dyn}(g)$ to $\bar{\epsilon}$. Our argument fails for smaller g , where the localization mechanism becomes more subtle (as discussed in Sec.III C the main text) and the first-order transition line is smeared into a chaotic crossover close to the mean-field critical point g_{dyn} . A similar fate happens to the second-order critical line, extending from the point $(g, J) = (g_{dyn}, 0)$, to finite values of J , so that the chaotic crossover prevents the possibility of a precise estimation of the tricritical point where the two lines meet. However, we can roughly identify the transition point as the center of the finite-width area where the two transition lines merge completely with the chaotic region: in the inset in Fig. 9 (bottom-right), we show that this happens approximately around $(g, J) \simeq (1.026, 0.17)$.

For $p = 4$, the results in Fig. 10 (right) show a discontinuous transition driven by J , this time detected by the time-averaged fluctuations $(\overline{\delta S^x})^2$, even though the semi-analytical estimation of $J_{dyn}(g)$ fails in this case. Moreover, here both the mean-field dynamical transition, driven by g , as well as the one driven by J , are of the first-order, so that we do not retrieve the tricritical behaviour discussed for $p = 3$.

-
- [1] A. Polkovnikov, K. Sengupta, A. Silva, and M. Vengalattore, Colloquium: Nonequilibrium dynamics of closed interacting quantum systems, *Reviews of Modern Physics* **83**, 863 (2011).
 [2] D. Rossini, A. Silva, G. Mussardo, and G. E. Santoro,

- Effective thermal dynamics following a quantum quench in a spin chain, *Phys. Rev. Lett.* **102**, 127204 (2009).
 [3] P. Calabrese, F. H. L. Essler, and M. Fagotti, Quantum quench in the transverse-field ising chain, *Phys. Rev. Lett.* **106**, 227203 (2011).

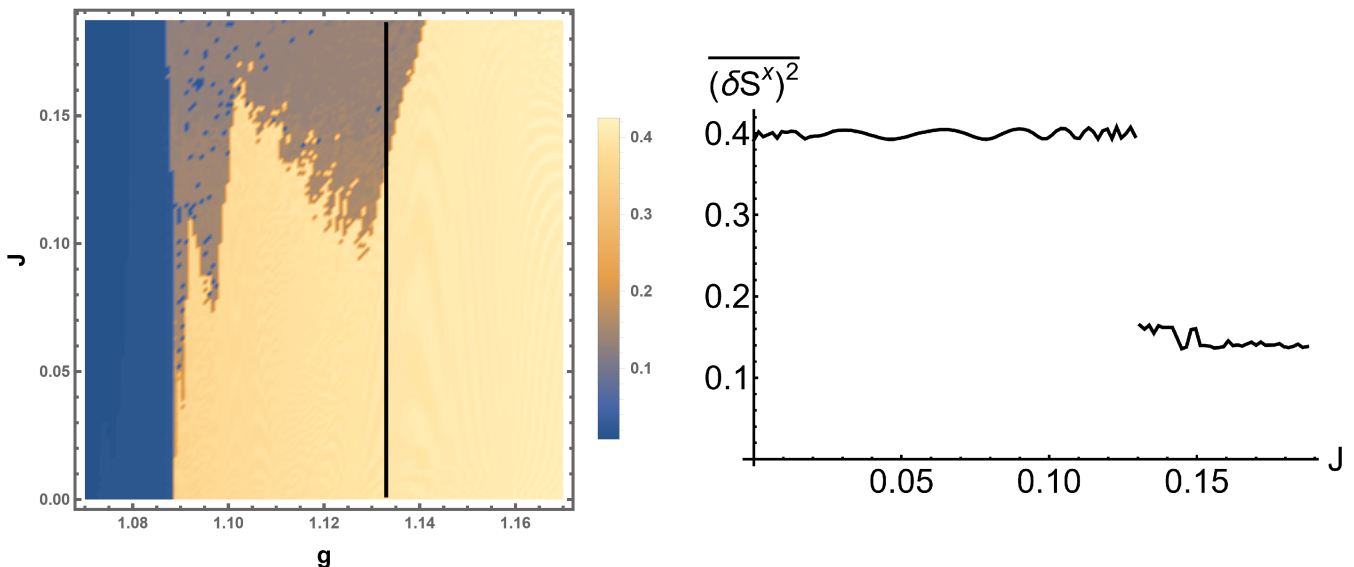


FIG. 10. (Color online) Non-equilibrium phase diagram for the p -spin model in eq. (1), for $p = 4$. **(Left)** Same phase diagram shown in Fig. 4 (left). The black vertical line and the green box indicate the values of g and J investigated in the plots on the right. **(Right)** Plot of the time-averaged fluctuations $\overline{(\delta S^x)^2}$, as function of J and at fixed $g \simeq 1.133$ (black line on the phase diagram on the left). $\overline{(\delta S^x)^2}$ is discontinuous around $J \simeq 0.131$.

- [4] A. Maraga, P. Smacchia, M. Fabrizio, and A. Silva, Nonadiabatic stationary behavior in a driven low-dimensional gapped system, *Phys. Rev. B* **90**, 041111 (2014).
- [5] A. Polkovnikov, Universal adiabatic dynamics in the vicinity of a quantum critical point, *Phys. Rev. B* **72**, 161201 (2005).
- [6] W. H. Zurek, U. Dorner, and P. Zoller, Dynamics of a quantum phase transition, *Phys. Rev. Lett.* **95**, 105701 (2005).
- [7] J. Dziarmaga, Dynamics of a quantum phase transition: Exact solution of the quantum Ising model, *Phys. Rev. Lett.* **95**, 245701 (2005).
- [8] R. W. Cherng and L. S. Levitov, Entropy and correlation functions of a driven quantum spin chain, *Phys. Rev. A* **73**, 043614 (2006).
- [9] S. Braun, M. Friesdorf, S. S. Hodgman, M. Schreiber, J. P. Ronzheimer, A. Riera, M. del Rey, I. Bloch, J. Eisert, and U. Schneider, Emergence of coherence and the dynamics of quantum phase transitions, *Proceedings of the National Academy of Sciences* **112**, 3641 (2015), <https://www.pnas.org/content/112/12/3641.full.pdf>.
- [10] M. Anquez, B. A. Robbins, H. M. Bharath, M. Boguslawski, T. M. Hoang, and M. S. Chapman, Quantum kibble-zurek mechanism in a spin-1 Bose-Einstein condensate, *Phys. Rev. Lett.* **116**, 155301 (2016).
- [11] L. W. Clark, L. Feng, and C. Chin, Universal space-time scaling symmetry in the dynamics of bosons across a quantum phase transition, *Science* **354**, 606 (2016), <https://science.sciencemag.org/content/354/6312/606.full.pdf>.
- [12] B. M. Anderson, L. W. Clark, J. Crawford, A. Glatz, I. S. Aranson, P. Scherpelz, L. Feng, C. Chin, and K. Levin, Direct lattice shaking of Bose condensates: Finite momentum superfluids, *Phys. Rev. Lett.* **118**, 220401 (2017).
- [13] S. Kang, S. W. Seo, J. H. Kim, and Y. Shin, Emergence and scaling of spin turbulence in quenched antiferromagnetic spinor Bose-Einstein condensates, *Phys. Rev. A* **95**, 053638 (2017).
- [14] A. Keesling, A. Omran, H. Levine, H. Bernien, H. Pichler, S. Choi, R. Samajdar, S. Schwartz, P. Silvi, S. Sachdev, P. Zoller, M. Endres, M. Greiner, V. Vuletić, and M. D. Lukin, Quantum kibble-zurek mechanism and critical dynamics on a programmable Rydberg simulator, *Nature* **568**, 207 (2019).
- [15] J.-M. Cui, F. J. Gómez-Ruiz, Y.-F. Huang, C.-F. Li, G.-C. Guo, and A. del Campo, Experimentally testing quantum critical dynamics beyond the kibble-zurek mechanism, *Communications Physics* **3**, 44 (2020).
- [16] T. Świsłocki, E. Witkowska, J. Dziarmaga, and M. Matuszewski, Double universality of a quantum phase transition in spinor condensates: Modification of the kibble-zurek mechanism by a conservation law, *Phys. Rev. Lett.* **110**, 045303 (2013).
- [17] I. B. Coulamy, A. Saguia, and M. S. Sarandy, Dynamics of the quantum search and quench-induced first-order phase transitions, *Phys. Rev. E* **95**, 022127 (2017).
- [18] K. Shimizu, T. Hirano, J. Park, Y. Kuno, and I. Ichinose, Out-of-equilibrium dynamics of multiple second-order quantum phase transitions in an extended Bose-Hubbard model: Superfluid, supersolid, and density wave, *Phys. Rev. A* **98**, 063603 (2018).
- [19] L. Del Re, M. Fabrizio, and E. Tosatti, Nonequilibrium and nonhomogeneous phenomena around a first-order quantum phase transition, *Phys. Rev. B* **93**, 125131 (2016).
- [20] A. Sinha, T. Chanda, and J. Dziarmaga, Nonadiabatic dynamics across a first-order quantum phase transition: Quantized bubble nucleation, *Phys. Rev. B* **103**, L220302 (2021).
- [21] G. Lagnese, F. M. Surace, M. Kormos, and P. Calabrese,

- False vacuum decay in quantum spin chains (2021), arXiv:2107.10176 [cond-mat.stat-mech].
- [22] L.-Y. Qiu, H.-Y. Liang, Y.-B. Yang, H.-X. Yang, T. Tian, Y. Xu, and L.-M. Duan, Observation of generalized kibble-zurek mechanism across a first-order quantum phase transition in a spinor condensate, *Science Advances* **6**, 10.1126/sciadv.aba7292 (2020), <https://advances.sciencemag.org/content/6/21/eaba7292.full.pdf> (2021).
- [23] M. Heyl, A. Polkovnikov, and S. Kehrein, Dynamical quantum phase transitions in the transverse-field ising model, *Phys. Rev. Lett.* **110**, 135704 (2013).
- [24] M. Heyl, Dynamical quantum phase transitions: a review, *Reports on Progress in Physics* **81**, 054001 (2018).
- [25] S. A. Weidinger, M. Heyl, A. Silva, and M. Knap, Dynamical quantum phase transitions in systems with continuous symmetry breaking, *Phys. Rev. B* **96**, 134313 (2017).
- [26] B. Žunkovič, M. Heyl, M. Knap, and A. Silva, Dynamical quantum phase transitions in spin chains with long-range interactions: Merging different concepts of nonequilibrium criticality, *Phys. Rev. Lett.* **120**, 130601 (2018).
- [27] J. C. Halimeh, V. Zauner-Stauber, I. P. McCulloch, I. de Vega, U. Schollwöck, and M. Kastner, Prethermalization and persistent order in the absence of a thermal phase transition, *Physical Review B* **95**, 10.1103/physrevb.95.024302 (2017).
- [28] J. Lang, B. Frank, and J. C. Halimeh, Dynamical quantum phase transitions: a geometric picture, *Phys. Rev. Lett.* **121**, 130603 (2018).
- [29] J. Lang, B. Frank, and J. C. Halimeh, Concurrence of dynamical phase transitions at finite temperature in the fully connected transverse-field ising model, *Physical Review B* **97**, 174401 (2018).
- [30] J. C. Halimeh and V. Zauner-Stauber, Dynamical phase diagram of spin chains with long-range interactions, arXiv preprint arXiv:1610.02019 (2016).
- [31] I. Homrighausen, N. O. Abeling, V. Zauner-Stauber, and J. C. Halimeh, Anomalous dynamical phase in quantum spin chains with long-range interactions, *Physical Review B* **96**, 104436 (2017).
- [32] B. Sciola and G. Biroli, Dynamical transitions and quantum quenches in mean-field models, *Journal of Statistical Mechanics: Theory and Experiment* **2011**, P11003 (2011).
- [33] P. Jurcevic, H. Shen, P. Hauke, C. Maier, T. Brydges, C. Hempel, B. P. Lanyon, M. Heyl, R. Blatt, and C. F. Roos, Direct observation of dynamical quantum phase transitions in an interacting many-body system, *Phys. Rev. Lett.* **119**, 080501 (2017).
- [34] A. Lerose, J. Marino, B. Žunkovič, A. Gambassi, and A. Silva, Chaotic dynamical ferromagnetic phase induced by nonequilibrium quantum fluctuations, *Phys. Rev. Lett.* **120**, 130603 (2018).
- [35] A. Lerose, B. Žunkovič, J. Marino, A. Gambassi, and A. Silva, Impact of nonequilibrium fluctuations on prethermal dynamical phase transitions in long-range interacting spin chains, *Physical Review B* **99**, 10.1103/physrevb.99.045128 (2019).
- [36] G. Piccitto, B. Žunkovič, and A. Silva, Dynamical phase diagram of a quantum ising chain with long-range interactions, *Phys. Rev. B* **100**, 180402 (2019).
- [37] G. Piccitto and A. Silva, Crossover from fast to slow dynamics in a long range interacting ising chain, *Journal of Statistical Mechanics: Theory and Experiment* **2019**, 094017 (2019).
- [38] E. Canovi, P. Werner, and M. Eckstein, First-order dynamical phase transitions, *Phys. Rev. Lett.* **113**, 265702 (2014).
- [39] P. Wang and R. Fazio, Dissipative phase transitions in the fully connected ising model with p -spin interaction, *Physical Review A* **103**, 10.1103/physreva.103.013306 (2021).
- [40] A. Rückriegel, A. Kreisel, and P. Kopietz, Time-dependent spin-wave theory, *Physical Review B* **85**, 10.1103/physrevb.85.054422 (2012).
- [41] B. Derrida, Random-energy model: Limit of a family of disordered models, *Phys. Rev. Lett.* **45**, 79 (1980).
- [42] B. Derrida, Random-energy model: An exactly solvable model of disordered systems, *Physical Review B* **24**, 2613 (1981).
- [43] T. Jörg, F. Krzakala, J. Kurchan, A. C. Maggs, and J. Pujos, Energy gaps in quantum first-order mean-field-like transitions: The problems that quantum annealing cannot solve, *EPL (Europhysics Letters)* **89**, 40004 (2010).
- [44] V. Bapst and G. Semerjian, On quantum mean-field models and their quantum annealing, *Journal of Statistical Mechanics: Theory and Experiment* **2012**, P06007 (2012).
- [45] A. Das, K. Sengupta, D. Sen, and B. K. Chakrabarti, Infinite-range ising ferromagnet in a time-dependent transverse magnetic field: Quench and ac dynamics near the quantum critical point, *Physical Review B* **74**, 10.1103/physrevb.74.144423 (2006).
- [46] M. Filippone, S. Dusuel, and J. Vidal, Quantum phase transitions in fully connected spin models: An entanglement perspective, *Phys. Rev. A* **83**, 022327 (2011).
- [47] M. H. Muñoz Arias, I. H. Deutsch, P. S. Jessen, and P. M. Poggi, Simulation of the complex dynamics of mean-field p -spin models using measurement-based quantum feedback control, *Phys. Rev. A* **102**, 022610 (2020).
- [48] Our discussion can be generalized to quenches in the transverse field starting from $g_0 > 0$, following the approach of Ref. [32].
- [49] J. Keeling, M. Bhaaseen, and B. Simons, Collective dynamics of bose-einstein condensates in optical cavities, *Phys. Rev. Lett.* **105**, 043001 (2010).
- [50] A. Gambassi and P. Calabrese, Quantum quenches as classical critical films, *EPL (Europhysics Letters)* **95**, 66007 (2011).
- [51] A. Dutta and J. Bhattacharjee, Phase transitions in the quantum ising and rotor models with a long-range interaction, *Physical Review B* **64**, 184106 (2001).
- [52] T. Mori, T. N. Ikeda, E. Kaminishi, and M. Ueda, Thermalization and prethermalization in isolated quantum systems: a theoretical overview, *Journal of Physics B: Atomic, Molecular and Optical Physics* **51**, 112001 (2018).
- [53] M. Gring, M. Kuhnert, T. Langen, T. Kitagawa, B. Rauer, M. Schreitl, I. Mazets, D. A. Smith, E. Demler, and J. Schmiedmayer, Relaxation and prethermalization in an isolated quantum system, *Science* **337**, 1318 (2012).
- [54] T. Langen, T. Gasenzer, and J. Schmiedmayer, Prethermalization and universal dynamics in near-integrable quantum systems, *Journal of Statistical Mechanics: Theory and Experiment* **2016**, 064009 (2016).
- [55] A. Auerbach, *Interacting electrons and quantum magnetism* (Springer Science & Business Media, 2012).

- [56] Notice that the right-hand side of eq. (14) is invariant under reflection $\phi \rightarrow \phi + \pi$ with respect to the z -axis, so that spin-wave emission are symmetric in the two wells for $p = 2$.
- [57] A. Vulpiani, F. Cecconi, and M. Cencini, *Chaos: from simple models to complex systems*, Vol. 17 (World Scientific, 2009).
- [58] See ancillary files *Animated plot p=3.mpeg* and *Animated plot p=4.mpeg*.
- [59] Here \mathbf{k} is a d -dimensional vector if the lattice has dimensionality $d > 1$.
- [60] Up to replacing all the terms in the form of $J\delta^{\alpha\beta}(t)$ with the more generic expression $\delta^{\alpha\beta}(t) \equiv \sum_{\mathbf{k} \neq \mathbf{0}} \Delta_{\mathbf{k}}^{\alpha\beta}(t) \tilde{J}_{\mathbf{k}}/(Ns)$.
- [61] Here, g_{sp} is p -dependent the value of the transverse field beyond which the effective potential displays a single paramagnetic well, as discussed also in Appendix A.